Lipidomics for diagnosis and prognosis of pulmonary hypertension

Natalie Bordag[1,2,3,15], Bence Miklos Nagy[2], Elmar Zügner[4], Helga Ludwig[5], Vasile Foris[2,6], Chandran Nagaraj[2,15], Valentina Biasin[2,7], Ulrich Bodenhofer[5], Christoph Magnes[4], Bradley A. Maron[8], Silvia Ulrich[9], Tobias J. Lange[10,11], Konrad Hötzenecker[12], Thomas Pieber[3,13,15], Horst Olschewski[2,6,15*], Andrea Olschewski[2,14,15]

Affiliations

[1]Department of Dermatology and Venereology, Medical University of Graz, Graz, Austria.

[2]Ludwig Boltzmann Institute for Lung Vascular Research, Graz, Austria.

[3]CBmed GmbH, Center for Biomarker Research in Medicine, Graz, Austria.

[4]Institute for Biomedical Research and Technologies (HEALTH), Joanneum Research Forschungsgesellschaft m.b.H, Graz, Austria.

[5]School of Informatics, Communications, and Media, University of Applied Sciences Upper Austria, Hagenberg, Austria.

[6]Division of Pulmonology, Department of Internal Medicine, Medical University of Graz, Graz, Austria.

[7]Division of Physiology, Otto Loewi Research Centre, Medical University of Graz, Graz, Austria.

[8]Division of Cardiovascular Medicine, Department of Medicine, Brigham and Women's Hospital and Harvard Medical School, Boston, Massachusetts, USA.

[9]Clinic of Pulmonology, University and University Hospital of Zurich, Zürich, Switzerland.

[10]Department of Internal Medicine II, Pulmonology and Critical Care, Kreisklinik Bad Reichenhall, Bad Reichenhall, Germany.

[11]Faculty of Medicine, University of Regensburg, Regensburg, Germany.

[12]Department of Thoracic Surgery, Medical University of Vienna, Vienna, Austria.

[13]Division of Endocrinology and Diabetology, Department of Internal Medicine, Medical University of Graz, Graz Austria.

[14]Experimental Anaesthesiology, Department of Anaesthesiology and Intensive Care Medicine, Medical University of Graz, Graz, Austria.

[15]BioMedTech, Graz, Austria.

*to whom correspondence should be addressed:

Prof. Horst Olschewski, Horst.Olschewski@medunigraz.at

Abstract

Pulmonary hypertension (PH) is a severe hemodynamic, progressive condition associated with high morbidity and mortality where early and less invasive diagnostics could crucially improve management. There is a need for biomarkers in PH that are functional, diagnostic, and prognostic. We used a broad metabolomics approach with machine learning analysis and specific free fatty acid (FFA)/lipid-ratios to develop diagnostic and prognostic PH biomarkers.

In a training cohort of 74 PH patients, 30 disease controls without PH, and 65 healthy controls, we identified diagnostic and prognostic markers that were validated in an independent cohort of 64 subjects. Markers based on lipophilic metabolites were more robust than those based on hydrophilic metabolites. FFA/lipid-ratios provided excellent diagnostic accuracy for PH with an AUC of up to 0.89 and 0.90 in the training and the validation cohorts, respectively. The ratios provided age-independent prognostic information and a combination of a ratio with established clinical scores increased the hazard ratio (HR) for FPHR4p and COMPERA2 from 2.5 to 4.3 and from 3.3 to 5.6, respectively.

Pulmonary arteries (PA) of idiopathic PAH (IPAH) lungs show lipid accumulation and altered expression of lipid homeostasis-related genes that may explain this accumulation. Our functional studies in PA endothelial and smooth muscle cells have shown that increased FFA levels caused excessive proliferation and PA endothelial barrier dysfunction, both hallmarks of pulmonary artery hypertension (PAH).

In conclusion, lipidomic changes in PH provide novel diagnostic and prognostic biomarkers and may point to new metabolic therapy targets.

Keywords

biomarker, prognosis, pulmonary hypertension, blood-based test, fatty acid to lipid ratio, lipidomics

Abbreviations

6MWD, six minute walking distance; ACh, Acetylcholine; ADMA, asymmetric dimethylarginine; AUC, area under the curve; BH, Benjamini–Hochberg; BMI, body mass index; BNP or NT-proBNP, natriuretic peptide levels; CO, cardiac output; COPD, chronic obstructive pulmonary disease; CI, cardiac index; CTEPH, chronic thromboembolic pulmonary hypertension; DC, diseased control (non-PH); DLCOcVA, diffusing capacity for carbon monoxide alveolar volume, hemoglobin corrected; ECAR; extracellular acidification rate; ECIS, electrical cell-substrate impedance sensor; FEV1, forced expiratory volumet 1 s; FVC, forced vital capacity; FFA, free fatty acids; H&E, hematoxylin-eosin; HC, healthy control; HILIC, hydrophilic interaction liquid chromatography; hPAEC, human pulmonary artery endothelial cells; hPASMC, human pulmonary artery smooth muscle cells; HILIC, hydrophilic interaction liquid chromatography; HR, hazard ratio; HRMS, high resolution mass spectrometry; ILD, interstitial lung disease; IPAH, idiopathic pulmonary arterial hypertension; iPCA, independent principal component analysis; IVD, *in vitro* diagnostics; LPC, lysophosphatidylcholine; LPE, lysophosphatidylethanolamine; LV, left ventricle; MAD, median absolute deviation; mPAP, mean pulmonary arterial pressure; MS, mass spectrometry; OCR; oxygen consumption rate; OPLS-DA, orthogonal projections to latent structures discriminant analysis; PA, pulmonary arteries; PAH; pulmonary arterial hypertension; PAP, pulmonary arterial pressure; PAWP, pulmonary arterial wedge pressure; PBS, phosphate-buffered saline; PC, phosphatidylcholine; PDGF, platelet-derived growth factor; PH, pulmonary hypertension; PPP, pentose phosphate pathway; PVR, pulmonary vascular resistance; QC, pooled from samples for quality control; RAP, right atrial pressure; RDW, red cell distribution width; RF, random forest; RHC, right heart catheterization; ROC, receiver operator curve; RT, room temperature (20 – 25 °C); SEM, standard error of mean; SM, sphingomyelin; SMA, smooth muscle actin; SvO2, mixed venous oxygen saturation; TAG, triacylglyceride; TEER, transendothelial electrical resistance; TLC, total lung capacity; VWF, von-Willebrand Factor; WHO FC, World Health Organization functional class; WU, wood unit; XGBoost, eXtreme Gradient Boosting;

Introduction

Pulmonary hypertension (PH) affects 1% of the world's population[1,2] and thus represents a significant global health problem. Even mild PH is a strong negative prognosticator in patients with left heart disease[3], lung disease[4], and pulmonary arterial hypertension (PAH)[5,6].

In recent decades, global research efforts have led to targeted therapies for the rare pulmonary vascular diseases PAH and chronic thromboembolic PH (CTEPH) caused by blood clots in the lung. Despite this, the estimated five-year survival rate for newly diagnosed PAH patients stagnates at only 61%[7,8].

Diagnosis of PH is challenging because measurement of pulmonary arterial pressure (PAP) requires right heart catheterization (RHC), whereas non-invasive methods provide only estimates of PAP[1] or are not widely available[9]. Natriuretic peptide levels (BNP or NT-proBNP) are the only recommended biomarker for PH, but they are not specific and even higher levels can be found in left ventricular (LV) diseases. Therefore, the development of new diagnostic tools for the detection of PH, risk stratification, and epidemiological studies remains an important issue[2].

Fibroproliferative remodelling of distal pulmonary arterioles drives elevation in pulmonary artery pressure and pulmonary vascular resistance in PH. This sequence is associated with unique metabolic changes as detected from plasma and magnetic resonance imaging studies[10–15] and vascular cells and matrix that increase the biomass of the vessel wall[16], which may be due to tryptophan, glutamine, and proline metabolites as well as changes in the lipid profile. Our hypothesis was that PH patients develop a characteristic metabolic profile that enables detection and risk stratification in PH groups 1, 2, 3 and 4 (ESC/ERS guidelines)[1]. We identified a unique lipidomic profile in a diverse PH cohort against healthy and diseased controls which was confirmed in an independent validation cohort. In addition, we show that the small pulmonary arteries (PA) are strongly affected by such lipidomic changes.

Results

Clinical and cardiopulmonary hemodynamic characteristics for the study cohorts

Our study included three classes of subjects: PH patients, healthy control subjects (HC) and lung disease controls (DC) without PH, all of whom underwent blood-based high resolution mass spectrometry (HRMS)-based metabolomics (see Fig. 1). PH patients had a mean PAP (mPAP) ≥ 25 mmHg and were either 1) PAH, 2) PH due to left heart disease (LV), 3) PH due to lung disease, or 4) CTEPH. All DC had mPAP < 25 mmHg with either metabolic syndrome, chronic obstructive pulmonary disease (COPD) or interstitial lung disease (ILD). The distributions in sex and body mass index (BMI) between PH and HC/DC were similar (see Fig. 1C). Age was in the same range, although controls tended to be younger. Metabolites were not significantly correlated with age (see Fig. S3).

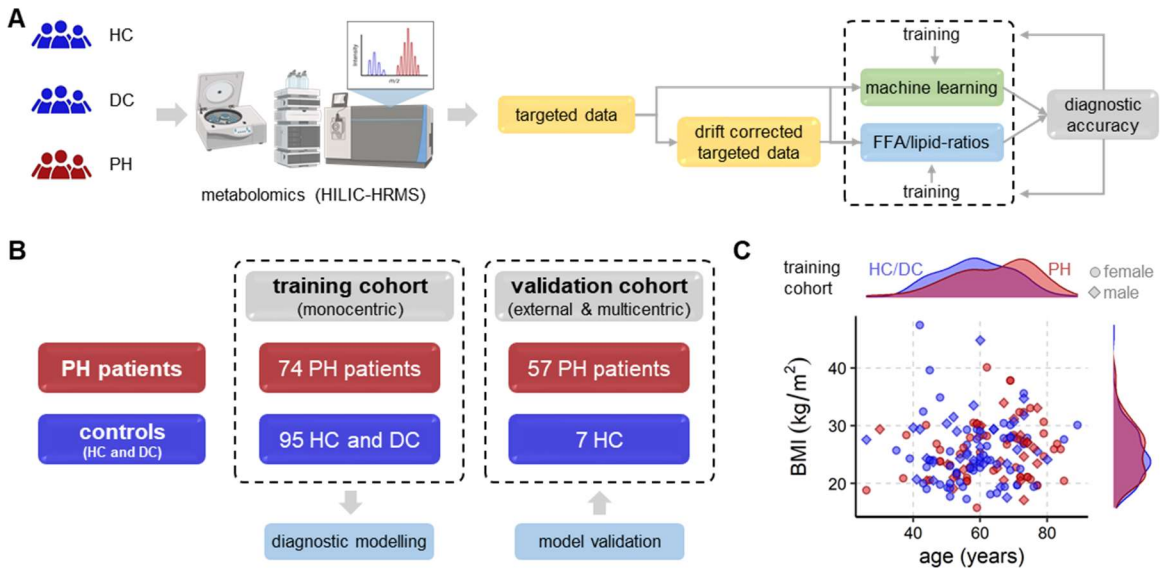

Fig. 1. Study overview for all cohorts. (A) Schematic workflow of metabolomics measurement and computational analysis. Created with BioRender.com. **(B)** Schematic overview of group distribution of all included patients (n = 233) in training and validation cohorts. **(C)** Scatter plot of BMI vs. age (shape of symbols by sex) in the training cohort with distribution histograms per PH and per HC/DC showing comparable distributions of sex and BMI in PH and HC/DC, avoiding potential confounders by design.

The training cohort consisted of PH patients, DC and HC, all sampled in Graz, Austria. The external validation cohort contained PH patients and HC from Zürich, Switzerland and Regensburg, Germany. Patient characteristics are summarized in Table 1.

119

120 **Table 1: Patients' characteristics (medians ± 95% confidence interval)**

	Training (n=169)			Validation (n=64)	
	HC (n=65)	DC (n=30)	PH (n=74)	HC (n=7)	PH (n=57)
Age, years	58.0±2.8	59.5±4.7	66.5±3.0	42.0±13.8	57.0±3.7
Female:male (ratio)	44:21 (2.1:1)	20:10 (2.0:1)	50:24 (2.1:1)	5:2 (2.5:1)	43:14 (3.1:1)
BMI (kg/m²)	24.1±0.9	26.2±3.0	25.9±1.1	21.0±1.7	26.3±1.4
Diagnosis (since years)	-	4.5±2.0	1.0±1.2	-	2.0±1.7
Pulmonary hemodynamics from RHC					
mPAP (mmHg) mean pulmonary arterial pressure	-	-	42.0±2.5	-	50.0±3.9
PAWP (mmHg) pulmonary arterial wedge pressure	-	-	10.0±1.3	-	9.0±0.9
CO (L/min) cardiac output	-	-	4.3±0.4	-	4.2±0.4
CI (L/min/m²) cardiac index	-	-	2.6±0.2	-	2.4±0.2
PVR (WU) pulmonary vascular resistance	-	-	7.1±1.0	-	9.1±1.7
RAP (mmHg) right atrial pressure	-	-	6.0±1.2	-	7.5±1.1
Clinical data					
6MWD (m) 6-min walk distance	-	454±41	330±34	-	403±28
WHO FC world health organisation functional class	-	2.0±0.2	3.0±0.2	-	2.0±0.2
FEV1 (% predicted) forced expiratory volume 1 s	-	51.5±9.9	75.0±5.6	-	82.2±3.0
FVC (% predicted) forced vital capacity	-	63.8±6.7	82.8±5.5	-	91.4±4.0
FEV1/FVC (% predicted)	-	56.3±8.5	74.4±3.0	-	75.7±2.1
TLC (% predicted) total lung capacity	-	103.0±10.8	94.0±3.9	-	96.5±3.5
DLCO cSB (% predicted) single-breath CO diffusing capacity, haemoglobin corrected	-	49.6±7.8	63.8±6.0	-	53.8±3.9
DLCO cVA (% predicted) diffusing capacity for CO alveolar volume, haemoglobin corrected	-	70.0±7.9	69.6±6.1	-	62.0±3.7
RDW (%) red cell distribution width	-	14.0±0.7	15.4±0.7	-	14.7±0.6
NT-proBNP (pg/mL)	-	90±41	869±806	-	751±475
Uric acid (mg/dL)	-	5.0±0.5	6.0±0.6	-	6.6±0.7
Creatinine (mg/dL)	-	0.80±0.09	1.02±0.12	-	1.00±0.23
Bilirubin total (mg/dL)	-	0.40±0.13	0.64±0.13	-	0.65±0.16

121 **Identification of a characteristic lipidomics profile in pulmonary hypertension**

122 The metabolome of patients was assessed with untargeted hydrophilic interaction liquid
123 chromatography (HILIC)-HRMS from serum, EDTA, and heparin plasma samples in four measurement

runs. As is typical with mass spectrometry (MS) based metabolomics methods, notable batch effects occurred between runs as well as drift within the longer runs (see Fig. S2). Drift correction was successfully performed (see Fig. S2) using quality control (QC) injections, which are a mix of equal sample volumes repeatedly measured to monitor instrument stability.

In total, 164 known metabolites were of consistent analytical quality suitable for multivariate and univariate exploratory analysis. Global metabolic changes were first examined using the unsupervised multivariate method independent principal component analysis (iPCA). The metabolomes of the PH patients differed from the control groups (HC and DC), which was visible as a clear group separation in the iPCA scores plot along the first component (x-axis, Fig. 2A). The observed metabolic difference was mainly driven by an increase in specific FFA in PH patients (Fig. 2B). The machine learning method orthogonal projections to latent structures discriminant analysis (OPLS-DA) confirmed that the observed global metabolic differences between PH and HC/DC were significant ($p < 0.001$, cross-validation and 1000 random permutations, Fig. 2C).

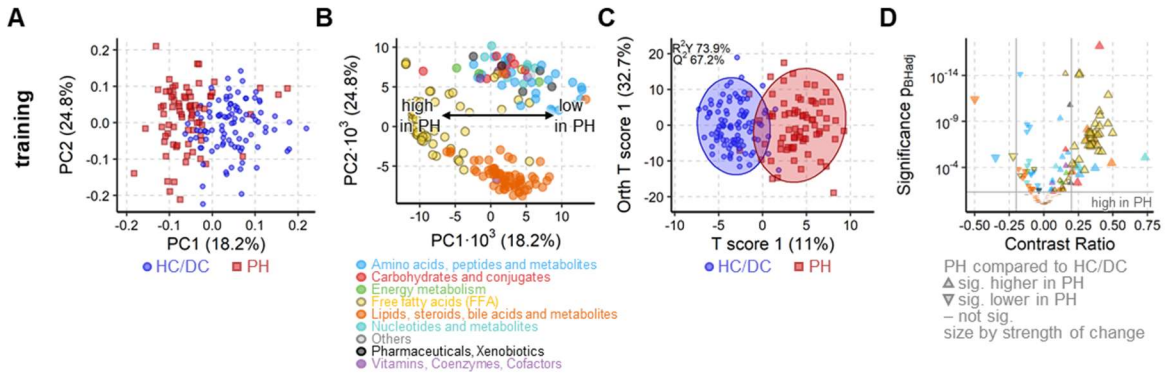

Fig. 2. PH is associated with a strong metabolic shift in the training cohort. (A) iPCA scores plot representing the metabolic profile of each subject as a dot. The proximity of the dots indicates the similarity of the subjects' metabolomes. Clear group separation by PH is visible along the first component. **(B)** Loadings plot corresponding to scores plot in (A). Each dot represents the contribution of the metabolite to the group separation observed in the scores plot. FFAs (yellow circles) strongly drive the group separation and are increased in PH patients. **(C)** OPLS-DA maximizes the group difference from PH to HC/DC and the resulting scores plot represents, as in A, the metabolome of each subject. Similarly, proximity indicates similarity and ellipses mark the 95% confidence interval of the groups. The difference between the metabolome of PH and HC/DC was significant ($Q^2 > 50\%$, $p < 0.001$ from 1000 random permutation). **(D)** Volcano plot of univariate analysis showing significant ($p_{BH} < 0.05$, grey horizontal line) and strong (absolute contrast ratio > 0.25, grey vertical lines) increase in FFAs (yellow triangles). For all methods A-D, 164 known metabolites from the training cohort samples (n = 169) were used (drift corrected, log_{10}-transformed data). Colors as in B.

The univariate statistical analysis confirmed that FFAs were strongly and significantly increased in PH compared with HC/DC (Fig. 2D). The few metabolites from routine clinical chemistry, e.g. uric acid, were strongly correlated with their respective HILIC-HRMS metabolites (Fig. S3). FFAs

140 and lipids were not strongly correlated with any clinical parameters known to be relevant to PH,
141 suggesting that the detected FFA changes may be independent from conventional clinical assessment.

142 **FFA/lipid-ratios diagnose pulmonary hypertension**

143 The potential of using metabolites to diagnose PH was first investigated with the machine
144 learning method random forest (RF)[17,18] and extreme gradient boosting (XGBoost)[19]. From the 164
145 metabolites, 11 were excluded from biomarker analysis because of low signal intensities and high noise
146 (see Supplementary Data 1). RF and XGBoost both achieved an area under the curve (AUC) of 0.83 in
147 the receiver operator curve (ROC) analysis in the validation set (Fig. 3A and Fig. S4). The drift
148 correction used here allowed a joint exploratory statistical analysis, but drift correction is impossible in
149 future routine clinical diagnostics. Therefore, all the diagnostic and prognostic performance was also
150 tested without drift correction. RF and XGBoost performance were almost equivalent without drift
151 correction, indicating that their nonlinear algorithms exhibit intrinsic drift-handling capabilities (Fig.
152 S4).

153 To find a technically simplified biomarker for PH, all metabolites were grouped according to
154 their chemical properties into hydrophilic metabolites and lipophilic FFAs & lipids. The performance
155 of hydrophilic metabolites alone was lower than that of FFAs & lipids alone. When all metabolites or
156 only the hydrophilic metabolites were used, the AUC of RF and XGBoost results dropped notably from
157 model training towards the external validation, regardless of the drift correction (Fig. 3B, C and Fig.
158 S4). However, for lipophilic metabolites, the AUC was much more consistent between training and
159 validation for both RF and XGBoost, suggesting that lipophilic metabolites were less susceptible to
160 technical problems and overfitting. Other important model performance parameters such as specificity,
161 sensitivity, and balanced accuracy were comparable for RF and XGBoost irrespective of drift correction
162 or metabolite selection (Fig. 3C). For RF and XGBoost, the average balanced accuracy was 71.5% and
163 70.6%, respectively, the specificity was 84.8% and 85.9%, respectively, and the sensitivity was 54%
164 and 50.7%, respectively (Fig. S4).

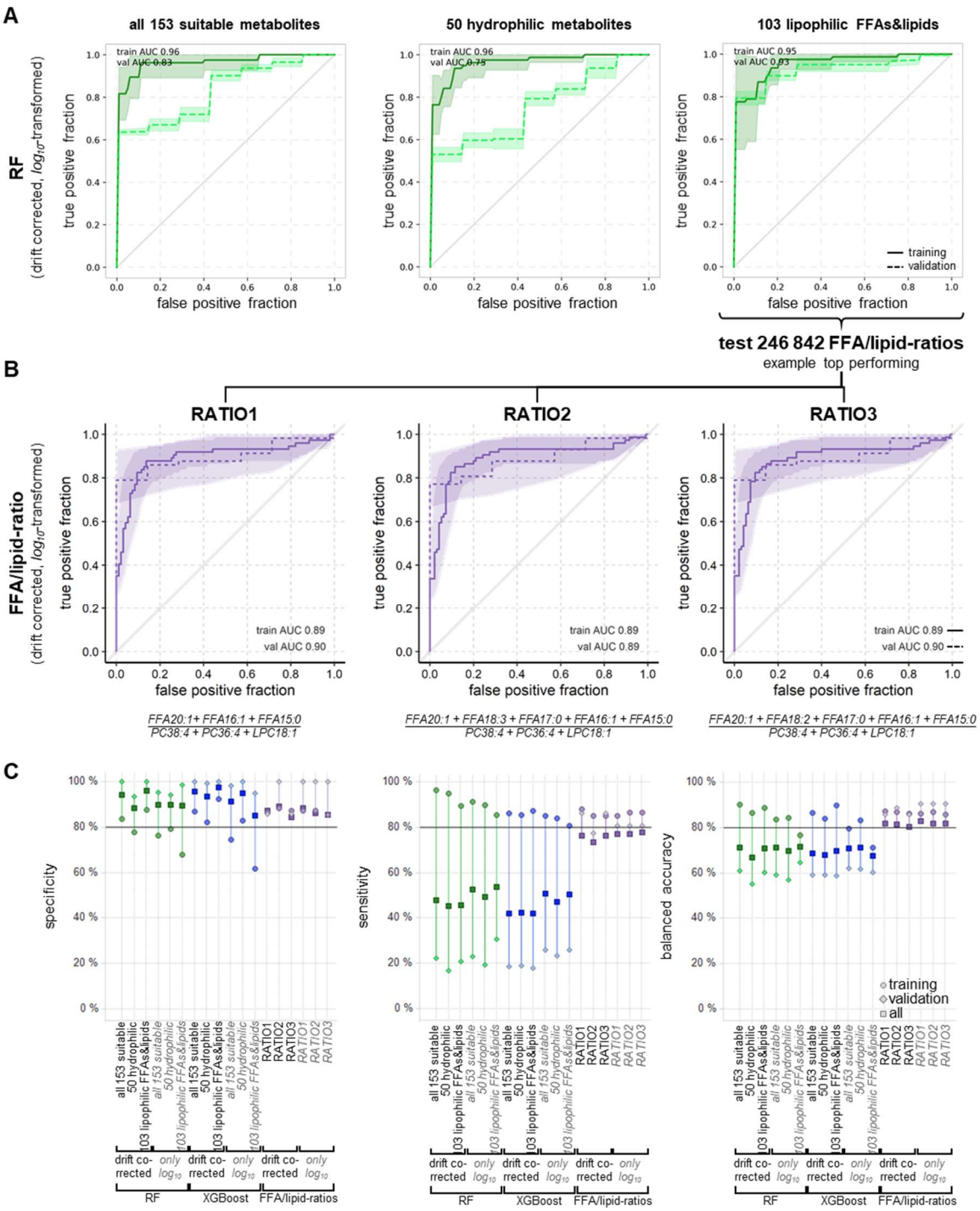

Fig. 3. Diagnostic accuracy for PH in training and validation cohorts. (A) ROC plots within the training cohort (n = 169, solid lines) and the validation cohort (n = 64, dashed lines) with their 95% confidence intervals as ribbons. For modelling, the training cohort was randomly split into 80% training and 20% testing data. The split was repeated five times without overlap of test data for cross-validation. RF used either all suitable 153 metabolites (left), only 50 hydrophilic metabolites (middle), or only 103 lipophilic metabolites (right) (drift corrected, log_{10}-transformed data). **(B)** The ROC plots of the three best FFA/lipid-ratios within the training cohort (n = 169, solid lines) and the validation cohort (n = 64, dashed lines) with their 95% confidence intervals as ribbons (drift corrected, log_{10}-transformed data). **(C)** Plot of model performance metrics sensitivity, specificity and balanced accuracy for RF, XGBoost, and the three best FFA/lipid-ratios when based on either training (circles) or validation (diamonds)

cohorts only or all available data (squares). The performance of RF and XGBoost was comparable for all three metabolite subsets with and without drift correction (both log_{10}-transformed). The performance of the three best FFA/lipid-ratios was more stable and balanced than of RF or XGBoost.

165 Next, we tested whether ratios built from lipophilic metabolites could replace machine learning
166 approaches to create an explainable, easy-to-measure marker with selected FFAs in the numerator and
167 selected lipids in the denominator. The FFAs in the numerator were selected based on their analytical
168 performance and statistical significance in PH versus HC/DC. The denominator was chosen to correct
169 for inter-personal differences in lipid metabolism using lipids without statistical significance in PH
170 versus HC/DC. For the nominator, 11 FFA were considered: FFA C15:0 (pentadecylic acid),
171 FFA C16:2 (palmitolinoleic acid), FFA C16:1 (palmitoleic acid), FFA C17:1 (heptadecenoic acid),
172 FFA C17:0 (margaric acid), FFA C18:3 (α-linolenic acid, ALA, or γ-linolenic acid, GLA), FFA C18:2
173 (linoleic acid, LA), FFA C18:1 (oleic acid), FFA C19:1 (nonadecenoic acid), FFA C20:5
174 (eicosapentanoic acid, EPA) and FFA C20:1 (eicosenoic acid). Eight lipids were considered for the
175 denominator: lysophosphatidylcholine (LPC) 18:2, LPC 18:1, phosphatidylcholine (PC 36:4, PC 38:6),
176 sphingomyelin (SM 34:2, SM 36:2), lysophosphatidylethanolamine (LPE) 16:0, and LPE 18:1. To
177 stabilize the ratios we also tested sums of up to six FFAs in the numerator and up to four lipids in the
178 denominator limiting the maximum number of individual metabolites in a given ratio to ten.

179 In total, about a quarter of a million FFA/lipid-ratios were created when systematically testing
180 all possibilities with ROC analysis. Most FFA/lipid-ratios achieved moderate to high performance with
181 AUCs above 0.8 (Fig. 3 and Fig. S5). In comparison, the diagnostic performance of each FFA was much
182 weaker with AUCs below 0.7. The diagnostic performance of the FFA/lipid-ratios was independent of
183 drift correction, making the FFA/lipid-ratios suitable for stand-alone routine measurements (Fig. S5).

184 There may be a concern that combining multiple metabolites in a ratio increases technical error
185 and impairs reproducibility. However, in our cohort, the calculated technical variability according to
186 the laws of error propagation was <5% for most FFA/lipid-ratios and <10% for all others (Fig. S5G).

187 For simplicity, the top three performing ratios were selected as examples by their performance
188 (highest AUC, sensitivity, specificity) and named RATIO1, RATIO2, and RATIO3 (Fig. S5). These
189 three ratios had six metabolites in common: numerator (FFA C20:1 + FFA C16:1 + FFA C15:0);
190 denominator (PC 38:4 + PC 36:4 + LPC 18:1). The only difference to RATIO1 was the addition of two
191 more FFA to the numerator sum (either FFA 18:3 + FFA 17:0 or FFA 18:2 + FFA 17:0, Fig. 3B) in
192 RATIO2 and RATIO3. The ROC curves of RATIO1-3 overlapped well between training and validation
193 cohort (Fig. 3B). All other important performance parameters were also very similar between RATIO1-
194 3 (Fig. 3C) and notably outperformed all machine learning models, irrespective of drift correction,
195 especially in terms of sensitivity with an average balanced accuracy of 85.5%, a specificity of 89.7%
196 and a sensitivity of 81.4% (Fig. 3C).

197 FFA/lipid-ratios massively reduce technical complexity compared to broad metabolomics runs
198 while achieving better diagnostic performance than machine learning approaches. Accordingly, we
199 believe that such FFA/lipid-ratios are suitable for future routine applications.

200 **Specific FFA/lipid-ratios predict survival**

201 The prognostic value of our RATIO1 was compared with well-established invasive and non-
202 invasive scores: FPHR4P[20] and COMPERA2[1,21]. Survival and hazard ratios (HR) were investigated for
203 all PH patients and patients with non-PH lung disease (COPD, ILD). For direct comparability of
204 Kaplan-Meier survival curves and HRs all numeric values were categorized into low or high risk
205 according to their optimal cut-off points (e.g. age 58 years).

206 We analysed two different survival times, one since sampling (ie, time of enrolment = baseline)
207 and one since PH diagnosis. Survival time since baseline was available for 129 PH and 21 DC (13
208 COPD, 8 ILD) patients, and time since diagnosis was available for 118 PH and 21 DC patients. The
209 COMPERA2 score was available for 121 PH and 20 DC patients, and the FPHR4p for 91 PH and 20
210 DC patients for times since baseline.

211 As expected, FPHR4p and COMPERA2 scores were significantly associated with survival time
212 since baseline (Fig. 4) and since diagnosis (Fig. S6). RATIO1 was also significantly associated with
213 survival (Fig. 4) with a similar HR to COMPERA2 scores. When RATIO1 was combined with each of
214 the scores (RATIO1 and score equally weighted), the prognostic value of the respective score improved
215 notably (Fig. 4). This indicates that our simple metabolomic marker provides independent prognostic
216 information and would complement established prognostic scores.

217 Next, we examined the major confounding factors age, sex and BMI. The HR for age alone was
218 significant for both survival since baseline and survival since diagnosis (Fig. S7). The HR for BMI
219 alone was only slightly elevated, whereas the HR for male sex was not significant. A joint model with
220 all three confounders showed that only age remained significant. Therefore, we included only age as
221 covariate to HR analysis of our RATIOs and the ratios and FPHR4p and COMPERA2 scores (Fig. S7).

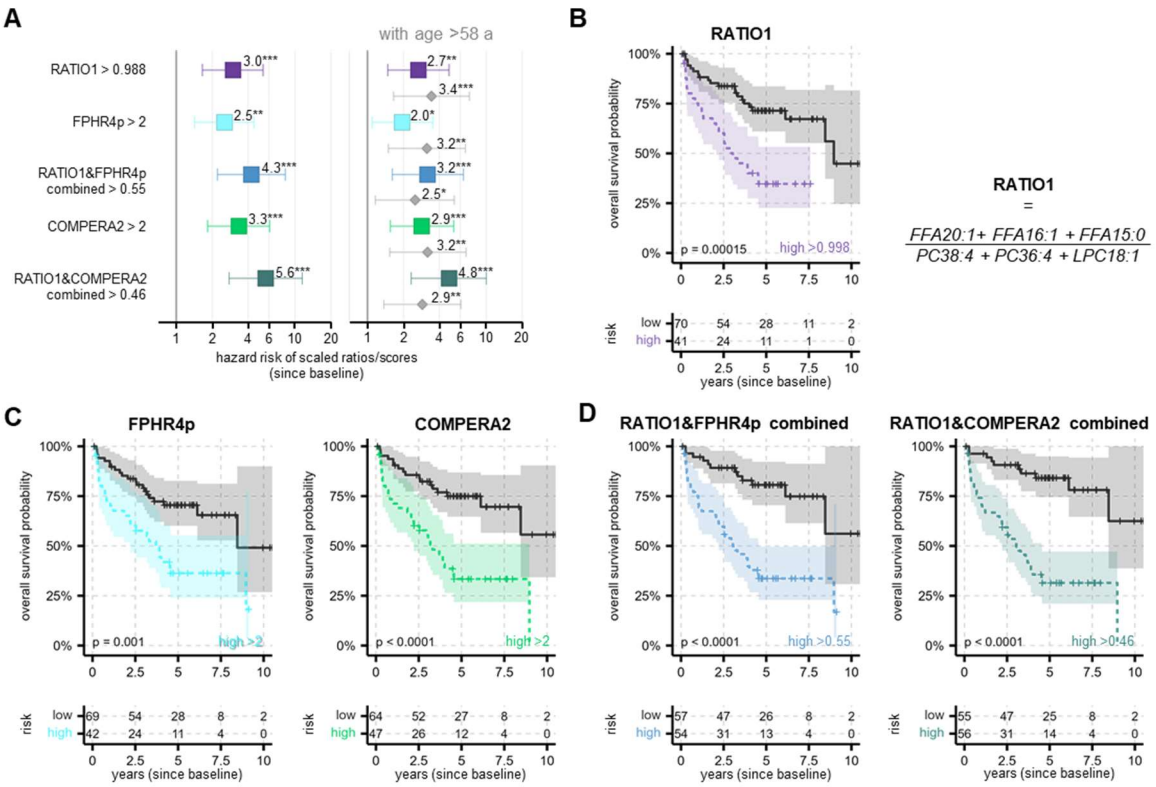

Fig. 4. RATIO1 predicts survival and improves prediction of established clinical scores. **(A)** Cox HR analysis for survival from baseline and 95% confidence intervals with statistical significance coded as not significant, (ns); * $p < 0.05$; ** $p < 0.01$; *** $p < 0.001$. Combining RATIO1 with FPHR4P or COMPERA2 increased HR compared with scores or RATIO1 alone. **(B, C, D)** Kaplan–Meier curves of survival from baseline by RATIO1 **(B)**, FPHR4p and COMPERA2 **(C)** and RATIO1 combined with FPHR4p or COMPERA2 **(D)**. All cut-offs were optimized with maxstat for both Cox HR analysis and Kaplan–Meier analysis. RATIO1 was based on log_{10}-transformed data without drift correction. RATIO1 and scores were combined scaled 0 to 1 to give equal weighing. FPHR4p was inverted so that higher scores also represent higher risk as in COMPERA2 for simpler interpretation.

The HR of RATIO1 remained similar and significant after correction for age (Fig. 4A). In contrast, correction for age decreased the respective HR for both FPHR4p and COMPERA2. This indicates that both FPHR4p and COMPERA2 scores may be are more age-dependent than RATIO1.

Finally, established clinical risk factors and single metabolites were analysed with respect to survival. Higher World Health Organization functional class (WHO FC), lower 6MWD, higher NT-proBNP and higher uric acid levels were associated with poorer survival (Fig. S8A). Survival analysis of each metabolite revealed that many metabolites were moderately associated with survival ($0.05 < p < 0.01$), but, with a much lower HR than FPHR4P, COMPERA2 or RATIO1. However, some metabolites strongly predicted survival, e.g. asymmetric dimethylarginine (ADMA) and N-acetylputrescine (Fig. S8A), which are well-known prognosticators in other diseases[22–24].

232 **Changes in lipid metabolism in pulmonary arteries of idiopathic PAH (IPAH) patients**

233 Because of the strong association between the lipidomics profile with PH, we investigated small
234 PA from IPAH patients (transplant recipients) and healthy donor lungs from explanted lungs. Oil red O
235 staining and co-staining with markers of endothelial and smooth muscle cells showed accumulation of
236 lipids in several IPAH PA (Fig. 5A). The observed lipid deposition could be the result of increased
237 uptake of fatty acids, dysregulation of fatty acid metabolism, or increased lipid synthesis. The observed
238 lipid deposition could be the result of increased uptake of fatty acids, dysregulation of fatty acid
239 metabolism, or increased lipid synthesis. Therefore, we performed laser-capture microdissection of
240 small PA (< 500 μm) from IPAH patients and healthy donors and examined gene expression of
241 transporters and enzymes related to lipid metabolism. Gene expression showed significant upregulation
242 of several key genes involved in lipid metabolism in IPAH (Fig. 5B). Most striking was the significant
243 upregulation of SLC27A5, GAPT1, AGAPT1, Lipin2 and DGAT1 in IPAH. DGAT1 plays a critical
244 role in lipid droplet formation. Up-regulation of the FFA transport protein SLC27A5 indicates increased
245 uptake of FFAs from the circulation. GPAT, AGPAT, and lipin family enzymes promote triglyceride
246 biosynthesis, incorporation of exogenous fatty acids into triacylglycerides (TAG) and phospholipids, as
247 well as β-oxidation. The upregulation of these genes in the small PAs of IPAH patients might represent
248 a compensatory mechanism for the increased circulating FFA levels or might be a manifestation of the
249 primary disease mechanism.

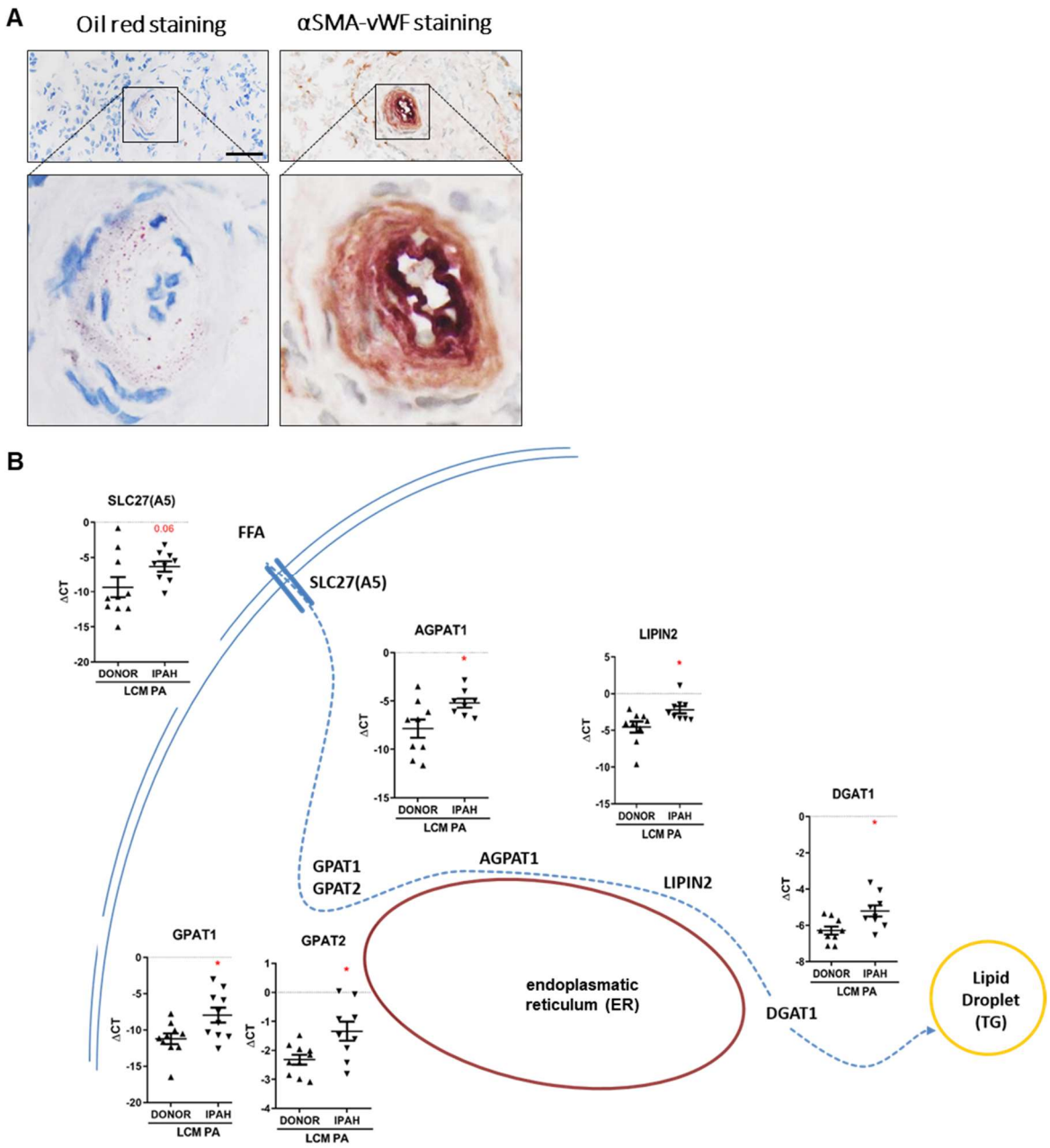

Fig. 5. Presence of lipids and expression of lipid-metabolism genes in IPAH pulmonary arteries. (A) Visualization of endothelium (von-Willebrand factor, VWF) and smooth muscle cell layer (smooth muscle actin, SMA) together with oil red staining in human IPAH lung serial sections (scale bar: 50 µm). **(B)** Gene expression of lipid homeostasis-related enzymes in laser-capture microdissected human PA (n = 8-10 independent patients, respectively). Vertical lines represent means with standard error of mean (SEM). Red asterisks mark Mann Whitney test < 0.05.

250 Next, we mimicked elevated circulating FFA levels by treating primary human pulmonary
251 artery smooth muscle cells (hPASMC) and human pulmonary artery endothelial cells (hPAEC) from
252 healthy donors with a FFA cocktail. Bodypi fluorescence staining showed accumulation of fat at the
253 cellular level in hPASMCs and hPAECs (Fig. 6A). To better understand the functional effects on the
254 cellular level, we performed further in-vitro studies with primary hPAEC and hPASMCs. In hPASMCs,

255 the treatment with a mixture of FFAs significantly promoted cell proliferation (Fig. 6B), and in hPAECs
256 significantly decreased acetylcholine (ACh)-induced NO secretion (Fig. 6C).

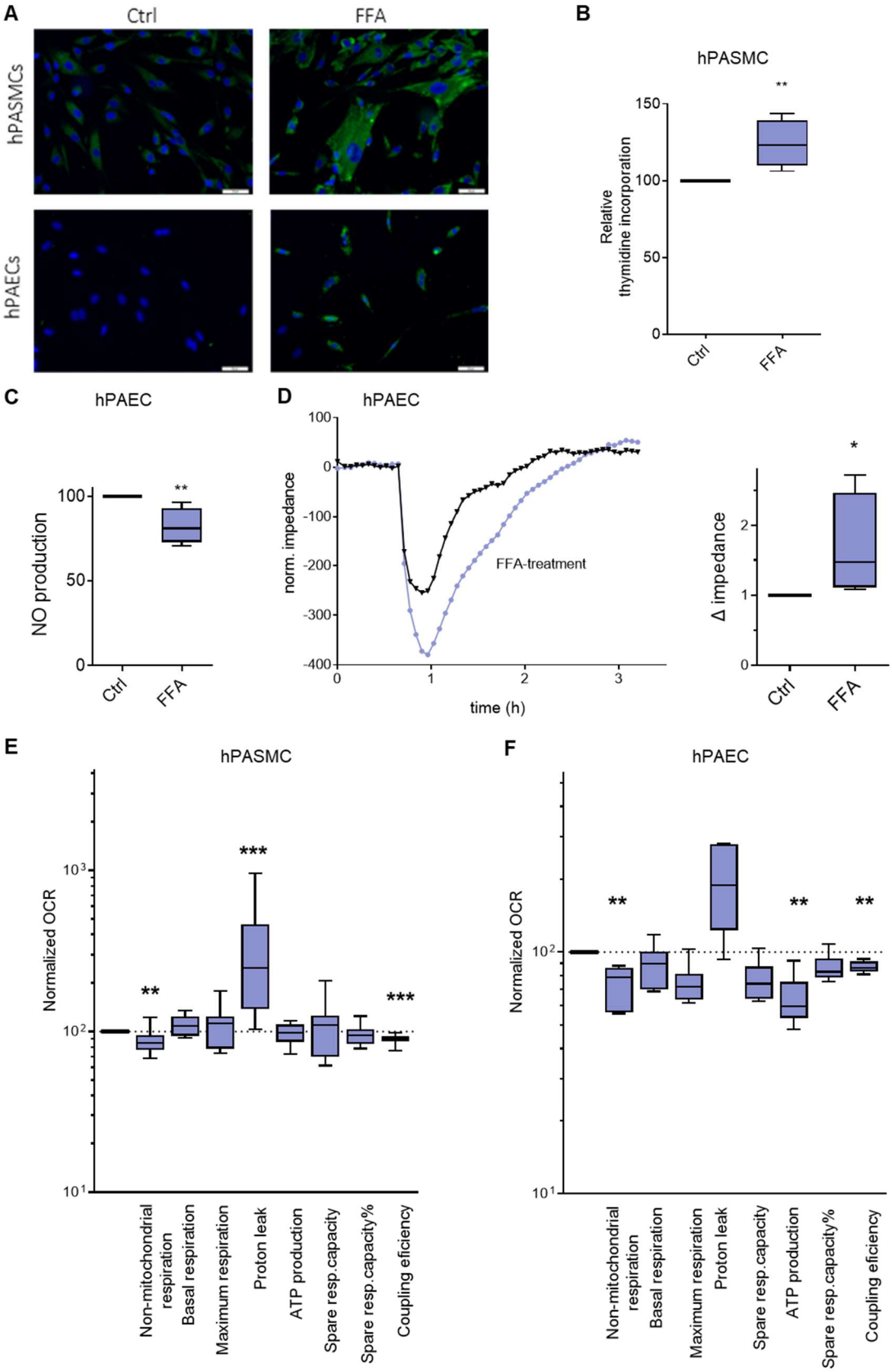

Fig. 6. Effects of FFA treatment on hPASMC and hPAEC. (A) Representative Bodipy fluorescence staining of hPASMC and hPAEC in the absence (Ctrl) or presence of FFA (scale bar: 50 µm). **(B)** Platelet-derived growth factor (PDGF)-BB induced proliferation of primary hPASMC measured with thymidine incorporation, in the absence (Ctrl) or presence of FFA (n = 4). Changes are expressed as percentages compared with untreated controls (Ctrl). **(C)** ACh-induced NO production in primary hPAEC (n = 4). Changes are expressed as percentages compared with untreated controls (Ctrl). **(D)** TEER, as determined by electrical cell-substrate impedance sensor (ECIS), shows a significant increase in hPAEC treated with FFA. Representative original curve (left panel) and changes expressed as percent change compared with controls (Ctrl) (n = 4). **(E, F)** Summarized data from hPASMC and hPAEC using the Seahorse XFe24 Extracellular Flux Analyzer. All measurements were performed on n = 25,000–50,000 cells/well and five wells per cell type. Each experimental group consisted of two to three patient cell lines (samples). All data were normalized to total protein per well before analysis. Results are given as median with interquartile range. Mann Whitney test * < 0.05, **< 0.01, ***< 0.001.

We investigated the effect of increased FFA levels on endothelial barrier function by determining the magnitude of thrombin-induced endothelial barrier dysfunction. Fig. 6D shows the typical response of control endothelium to thrombin. When endothelial monolayers were pre-treated with FFA they exhibited a significantly pronounced decrease in transendothelial electrical resistance (TEER) and delayed recovery of barrier function compared to control media (Fig. 6D). These observed effects upon FFA treatment all suggest increased barrier dysfunction. Finally, we examined FFA-induced metabolic responses in hPASMCs and hPAECs and found significantly decreased coupling efficiency in both cell types in response to FFA treatment (Fig. 6E, F). Moreover, FFA exposure decreased non-mitochondrial respiration and ATP production in hPAEC and increased proton leak in hPASMC. These results show that healthy hPASMCs and hPAECs, under FFA treatment, develop phenotypic changes that have been described as characteristic of IPAH. This suggests that high concentrations of circulating FFAs may deteriorate the maintenance function of the endothelium and simultaneously cause dysfunction of the smooth muscle layer of the small PA, representing either a primary cause or a novel vicious circle in PH.

Discussion

To our knowledge, this study is the first to apply unsupervised, broad metabolome analysis of PH patients of group 1 to 4. The generated specific FFA/lipid-ratios accurately identified patients with PH and predicted prognosis, independent of existing clinical prognostic scores and age. Their diagnostic and prognostic value was validated in an independent international cohort. Furthermore, *in vitro* mechanistic studies confirmed the disturbed lipid metabolism in PA of IPAH patients and the adverse effects of elevated FFA on hPAEC and hPASMC homeostasis. Our simple FFA/lipid-ratios might be useful in the diagnosis and clinical management of PH patients and might serve as surrogate end points in future clinical trials.

281 Although there has been tremendous progress in the understanding of PAH in recent decades,
282 there is still an unmet need for therapy. According to a recent literature review, the five-year survival
283 rate for newly diagnosed patients has not significantly increased despite a multitude of approved PAH
284 medications[8]. This may be due to the fact that the initial phase of the disease is clinically silent and
285 sensitive diagnostic methods are missing. PAH affects all aspects of a person's daily life and has a
286 major impact on quality of life, including physical activity, well-being and emotional and social
287 functioning[25], where even a mild elevation in PAP may limit patients' exercise capacity and reduce life
288 expectancy[1,5,6,26]. Thus, it is crucial to identify novel, simple biomarkers for early identification and risk
289 stratification, preferably based on the cellular and molecular mechanisms underlying the disease, to
290 determine prognosis, initiate treatment, and monitor response and long-term disease progression.

291 Spanning over two decades, extensive basic, translational, and clinical analyses have supported
292 a causative link between metabolic reprogramming and PAH[27]. Similar to the Warburg effect in cancer,
293 a shift from mitochondrial oxidation to glycolysis appears to occur in the right ventricle of PAH
294 patients[28,29]. In this study, we show that the small PAs are also affected by significant metabolic changes.
295 Taking cues from cancer, recent data demonstrate significant alterations in metabolic programs other
296 than glycolysis and glucose oxidation, including the pentose phosphate pathway (PPP), glutaminolysis,
297 lipolysis, fatty acid synthesis and oxidation and changes in the plasma proteome [12–16,30,31]. However, it
298 remains unclear whether these changes originate in the overloaded right ventricle, in the primarily
299 affected pulmonary vessels, or elsewhere.

300 In our cohort, severe metabolic perturbations were detected using an open metabolomics
301 approach, but the most severe and consistent changes were found in FFAs. Classical machine learning
302 using RF and XGboost showed that these metabolic differences held a high potential for diagnostic
303 biomarkers. Furthermore, these approaches were able to overcome typical technical MS-specific
304 problems such as batch effects and intensity jumps between measurements, which usually require drift
305 correction. The performance of RF and XGBoost models was independent of drift correction which is
306 obviously due to their nonlinear algorithms.

307 These strong metabolic perturbations are valuable for diagnostic and prognostic purposes,
308 particularly in the form of an easily applicable FFA/lipid-ratio. In order to be implemented in routine,
309 such diagnostics must deliver reliable results at all times independent of batch effects and drift
310 corrections. However, since absolute quantitative methods are labour intensive and costly, we tested
311 whether ratios of measured parameters provide an intra-sample normalization as a possible solution.
312 We used ratios of selected FFAs and lipids with the rationale that lipid levels correct for both batch
313 effects and inter-individual variability of patients' lipid metabolism and lifestyle. Technically, the
314 similar polarity of lipids and FFAs should help reduce the complexity and cost of high-throughput
315 measurements.

316 These FFA/lipid-ratios performed very well in both PH diagnosis and survival prediction and
317 were also independent of batch effects. The diagnostic performance of these FFA/lipid-ratios even
318 outperformed RF and XGBoost models, especially in sensitivity. In addition, the results were stable
319 despite the use of different sample types such as serum, heparin and EDTA plasma from three centres;
320 a very important factor for broad applicability in routine diagnostics. The FFA/lipid-ratios are easy to
321 use and fully explainable compared to machine learning models, which is advantageous for future
322 studies and regulatory approval processes for *in vitro* diagnostics (IVD).

323 Survival prediction is an important tool in the management of PAH patients. Several clinical
324 scores have been established, with FPHR4P and COMPERA2 representing most recent developments
325 derived from large databases[20,21]. The FPHR4P[20] score estimates prognosis based on WHO FC, 6MWD,
326 CI, and RAP, while COMPERA2[21] is based on non-invasive parameters (WHO FC, 6MWD, NT-pro-
327 BNP). In our cohort, both scores predicted survival but lost some predictive power when corrected for
328 age. In contrast, our RATIO1 predicted survival more independently of age. Most importantly, both
329 clinical scores gained predictive power when combined with RATIO1. Thus, FFA/lipid-ratios represent
330 an independent prognostic factor that combines favourably with established prognostic PH scores.

331 The uptake and metabolism of long-chain fatty acids is critical for many physiological and
332 cellular processes, and cellular accumulation may cause numerous pathological and functional changes.
333 Previous investigations of PAH have shown severe metabolic changes of the right ventricle and elevated
334 *in vivo* myocardial triglyceride content[10,28,29]. Our investigations add important information by showing
335 that small PA of IPAH patients were affected by lipid accumulation. Interestingly, we found increased
336 gene expression of enzymes responsible for fatty acid uptake and triglyceride biosynthesis in these
337 vessels (Fig. 5C). This could be caused by the high FFA levels in the circulation, however, it could also
338 represent a primary change in the cell physiology that deteriorates PH. The present data suggest that in
339 PH, the failing right ventricle is no longer able to metabolise FFAs, leading to an increase of circulating
340 FFA levels, which negatively affects pulmonary vascular cells. However, it is also possible that there
341 are primary changes in the lipid metabolism of the small PAs or elsewhere, which then lead to altered
342 cellular function, subsequently increasing right ventricular afterload and initiate a vicious circle in PH.

343 Numerous studies have indicated that the expression levels of GAPT1 / AGPAT1 / lipin-1 have
344 important cellular metabolic consequences[32–35]. This might explain some of the functional changes in
345 IPAH endothelial cells and hPASMC after FFA exposure compared with controls. For the first time,
346 we explored the effects of FFA exposure in primary human hPAECs and hPASMCs. FFA exposure
347 decreased NO secretion and impaired barrier function in hPAECs, while proliferation increased in
348 hPASMC. In addition, exposure to FFAs induced changes in non-mitochondrial respiration and
349 coupling efficiency in both cell types. These results provide evidence for impaired lipid handling in
350 IPAH PAs that might even trigger the remodelling in PAH.

351 Strengths of this study include the broad metabolomics approach, sampling and processing
352 conditions as in routine clinical practice, inclusion of a disease control group, comprehensive clinical
353 assessment, use of machine learning, development of diagnostic and predictive FFA/lipid-ratios, and
354 mechanistic studies in primary IPAH PA cells. The disadvantage of a comparatively modest number of
355 participants, particularly the number of controls in the validation cohort, was offset by well standardized
356 clinical characterization, including RHC, coupled with long follow-up times that enable survival
357 analysis.

358 Our blood samples were collected along with clinical routine blood draws, demonstrating that
359 it is not necessary to sample under strictly controlled conditions for obtaining specific FFA/lipid-ratios.
360 All metabolic measurements were based on high-resolution mass spectrometry, a very sensitive and
361 exact method, yet slow, expensive and work-intensive. However, our FFA/lipid-ratios were based on a
362 very simplified approach to characterize the metabolic derangement. The combination of
363 FFA/lipid-ratios with established FPHR4P and COMPERA2 scores was not optimized, since our main
364 focus was to find new, independent diagnostic and prognostic biomarkers but still provided clear results.

365 Future studies should include larger numbers of patients with a balanced group distribution and
366 more patients with early pulmonary hypertension with less impairment of right ventricular function.
367 Future longitudinal studies are also warranted to investigate the value of metabolic markers for patient
368 management.

369

370 **Conclusions**

371 Our FFA/lipid-ratio, based on overt lipid changes in PH patients, identified PH patients with a
372 high accuracy and was associated with prognosis. If implemented into the management strategy for PH
373 patients, this could inform therapy decisions to improve outcomes. Mechanistic insights into the
374 metabolic changes in small PA could identify new therapeutic targets.

375 # Online Methods

376 **Cohort Data Sources**

377 Results from the Graz Pulmonary Hypertension Registry (GRAPH) have been reported
378 previously[36,37]. Briefly, the program uses a software application linked to the electronic health record
379 for documentation of all patients of the Division of Pulmonology at the Department of Internal Medicine
380 of the Medical University of Graz who gave written informed consent. Demographic, clinical,
381 echocardiographic, procedural, and hemodynamic data and blood samples are collected and tracked for
382 longitudinal outcomes. All hemodynamics were measured in a standardized fashion by the same
383 experienced team[36]. Regularly scheduled quality checks of the registry are performed to ensure
384 completeness and accuracy. Written informed consent was obtained from all patients and the study was
385 conducted in line with the Helsinki declaration. The study was approved by the institutional ethics board
386 (identifier: 23-408ex10/11), and the study has been registered at ClinicalTrials.gov (NCT01607502).

387 The BioPersMed (Biomarkers of Personalised Medicine) project is designed as a single-centre,
388 prospective, observational cardiovascular risk study. Between 2010 and 2016, 1022 community
389 dwelling and asymptomatic individuals were regionally recruited and assessed biannually including a
390 standardized biospecimen acquisition[38]. Written informed consent was obtained from all patients and
391 the study was conducted in line with the Helsinki declaration.

392 **Cohort Study Population**

393 We retrospectively enrolled two consecutive cohorts of patients identified through our single-
394 centre GRAPH registry and labelled them as GRAPH-Metabolomics (GRAPH-M).

395 The inclusion criteria for the first cohort were diagnosis of idiopathic pulmonary arterial
396 hypertension (IPAH) and absence of severe co-morbidities. Healthy sex- and age-matched subjects
397 served as a healthy controls (HC).

398 Inclusion criteria for the second cohort consisted of the following PH groups 1 – 4: 1) PAH, or
399 2) PH associated with heart disease, 3) PH associated with lung diseases (COPD, ILD), or 4) CTEPH.
400 This cohort of disease controls (DC) consisted of patients with airway or parenchymal lung disease or
401 patients with metabolic syndrome (hypertension, hypercholesterinemia and type 2 diabetes mellitus)
402 but no signs of elevated PAP. Healthy sex- and age-matched subjects served as a control group (HC).
403 The patients with the metabolic syndrome were selected from the BioPersMed cohort Graz.

404 All cohorts with the exception of patients with metabolic syndrome or HC underwent RHC. In
405 patients who underwent multiple RHCs, the first RHC was considered the index procedure and was the
406 only one included in the analysis. Patients were included in the analyses if data from a complete RHC
407 were available, including a resting value for mPAP, PAWP, CO, heart rate, systolic and diastolic PA

408 pressure, PVR and mixed venous oxygen saturation (SvO_2). We used the standard equation to calculate
409 the pulmonary vascular resistance with PVR = (mPAP - PAWP)/CO expressed in WU.

410 **Validation Cohort**

411 This cohort comprised an international multicentric patient cohort. The inclusion criteria for the
412 validation cohort were the confirmed diagnosis of PAH and informed written consent at the home
413 institution. All participating centers were experienced centers of excellence for PH and all patients
414 underwent RHC in a standardized manner. Demographic, clinical, echocardiographic, procedural, and
415 hemodynamic data and blood samples were available as anonymized data. The sample collection was
416 approved by the local Ethics Committee in each local center (Regensburg University, ethics committee
417 No. 08/090 and cantonal ethical review board Zürich KEK 2010-0129; 2014-0214; 2017-0476).

418 **Cohort Outcomes**

419 The primary outcome was the confirmation of PH, defined as mPAP ≥ 25 mmHg according to
420 the ERS/ESC guidelines from 2015[39]. The secondary endpoints included time to all-cause mortality
421 with data provided by Statistic Austria (single-centre registry Graz) and by the respective centers who
422 contributed to the validation cohort. A complete list of covariates analyzed in this study is provided in
423 the Supplementary Material (Fig. S3).

424 **Human lung tissue samples**

425 Human lung tissue samples were obtained from patients with IPAH who underwent lung
426 transplantation at the Department of Surgery, Division of Thoracic Surgery, Medical University of
427 Vienna, Vienna, Austria. The protocol and tissue usage were approved by the institutional ethics
428 committee (976/2010) and written patient consent was obtained before lung transplantation. The patient
429 characteristics included: age at the time of the transplantation, weight, height, sex, mPAP measured by
430 RHC, pulmonary function tests, as well as the medical therapy. The chest computed tomography scans
431 and RHC data were reviewed by experienced pathologists and pulmonologists to verify the diagnosis.
432 Healthy donor lung tissue was obtained from the same source. Donor/IPAH patient characteristics are
433 given in Supplementary Material (Table S2).

434 **Lung histological Oil Red O staining**

435 The lipid accumulation of lung tissues was visualized by Oil Red O staining (Merck KGaA,
436 Darmstadt, Germany). Lung tissue was embedded in tissue freezing medium, were snap frozen at
437 −80 °C and sliced using a Leica CM 1900 cryostat (Leica Biosystems GmbH, Wetzlar, Germany) at a
438 thickness of 5µm per section. The slices were stained with Oil Red O working solution for 10 min,
439 differentiated in isopropanol for 5 min, and then washed with water at room temperature (20 – 25 °C)
440 (RT). The experiments were finished according to the manufacturer's instructions. The morphological

441 features of the tissues were assessed by hematoxylin-eosin (H&E) staining. The lipid in the tissue
442 observed by microscope.

443 **Laser capture microdissection of PA and RNA extraction**

444 Laser capture microdissection (LCM) of 10 donor lungs and 10 lungs from IPAH patients, as
445 well as mRNA isolation and cDNA synthesis were performed as previously described[40]. The intima and
446 media layers of PAs of 100 – 500 µm diameter were selected, marked and isolated with the Arcturus®
447 LCM System. Captured vessels were immediately transferred into RNA lysis buffer and were snap
448 frozen. RNeasy Micro Kit was utilized to isolate RNA (RNeasy Micro Kit, Qiagen, Hilden, Germany)[41].

449 **qRT-PCR - laser capture microdissected human PA**

450 The expression of enzymes and transporters was analyzed with real-time quantitative (qRT)-
451 PCR using the QuantiFast SYBR PCR reagent (Qiagen, Hilden, Germany) according to[42]. Primer pairs
452 (Eurofins, Graz, Austria), summarized in Supplementary Material (Table S3), were designed to span at
453 least one exon-exon boundary to avoid the amplification of genomic DNA. The specificity of all
454 primers, as well as the length of the amplicon, were confirmed by melting curve analysis and by running
455 the products on 2% agarose gels, respectively.

456 **Cell Isolation and culture**

457 ***hPAECs***

458 hPAECs were either purchased from Lonza or isolated from donor lungs. For the isolation of
459 donor hPAECs, PA (< 2 mm in diameter) were isolated and the endothelium incubated with an
460 enzymatic mixture of collagenase, DNAse and dispaze in HBSS at RT[43]. Cell suspension was collected,
461 resuspended in VascuLife Complete SMC Medium and cultured in gelatin-coated T25 flasks at 37°C
462 and 5% CO_2. After reaching 70 – 80% confluency, cells were trypsinized, enriched by 3 consecutive
463 steps of CD31-selective magnetic-activated cell sorting technology and verified via morphological and
464 marker confirmation (smooth muscle actin SMA, fibronectin, vimentin, von-Willebrand Factor VWF,
465 smooth muscle myosin heavy chain and CD31). Surplus hPAECs were frozen (endothelial cell complete
466 medium containing 12% FCS and 10% DMSO) and stored in liquid nitrogen until further use. Passages
467 2–6 were used for the experiments. Detailed patient characteristics of isolated hPAECs can be found in
468 Supplementary Material (Table S4).

469 ***hPASMCs***

470 The isolation and culture of human hPASMCs was performed as previously reported[44]. After
471 the removal of the endothelial cell layer, the media was peeled away from the underlying adventitial
472 layer and cut into approximately 1–2 mm^2 sections, centrifuged and resuspended in VascuLife

473 Complete SMC Medium supplemented with 20% FCS and 0.2% antibiotics, then transferred to T75
474 flasks and cultured at 37°C and 5% CO_2. After a confluent monolayer of hPASMC had formed, the
475 cells were trypsinized and either cultured in VascuLife Complete SMC medium supplemented with
476 10% FCS and 0.2% antibiotics, or frozen (VascuLife Complete SMC Medium containing 15% FCS and
477 10% DMSO) and stored in liquid nitrogen until further use. Passages 4–8 were used for the experiments.
478 Detailed patient characteristics of isolated hPASMCs can be found in Supplementary Material (Table
479 S4).

480 **Lipid visualized by bodipy staining**

481 BODIPY (D3922, Invitrogen, Carlsbad, Calif, USA) (excitation wavelength 493 nm, emission
482 maximum 503 nm), was diluted in phosphate-buffered saline (PBS, 137 mM NaCl, 2.7 mM KCl, 12
483 mM $HPO_4^{2-}/H_2PO_4^-$, pH 7.4) or DMSO at a concentration of 1 mg/mL and applied to the hPASMCs
484 and hPAECs for 20 mins at RT. Fixed cells (4% paraformaldehyde at 37°C for 5 mins) were used.
485 Following fixation, samples were washed 3 times in PBS for 10 mins. Sections were counterstained
486 with 4′,6-diamidino-2-phenylindole dihydrochloride (DAPI; Sigma-Aldrich) to visualize nuclei and
487 covered with glass cover slips. Images were taken using a laser scanning confocal microscope (Zeiss
488 LMS 510 META; Zeiss, Jena, Germany) with Plan-Neofluar (×40 /1.3 Oil DIC) objective.

489 **Measuring cell metabolic state**

490 Oxygen consumption rate (OCR) and extracellular acidification rate (ECAR) were determined
491 by the Seahorse XFp analyzer (Agilent, USA)[45]. hPASMCs or hPAECs were plated onto cell culture
492 microplates on the day before the experiments and treated with 0.25mM FFA (a mix of oleate, FFA
493 16:0 and FFA C18 (2:1:1)) in VascuLife® complete Medium and incubated for 24 h. Cells were then
494 incubated in XF assay medium (Agilent), supplemented with 25 mmol/L glucose and 1 mmol/L
495 pyruvate (hPASMCs) or 10 mmol/L glucose, 1 mmol/L pyruvate, and 2 mmol/L L-glutamine (hPAECs)
496 for 1 h at RT before the measurement. After the recording of the basal rates of OCR and ECAR, final
497 concentrations of 1 μmol/L oligomycin, 1 μmol/L carbonyl cyanide-4 (trifluoromethoxy)
498 phenylhydrazone, and 0.5 μmol/L rotenone and antimycin A for human hPASMCs; 1 μmol/L
499 oligomycin, 1 μmol/L carbonyl cyanide-4 (trifluoromethoxy) phenylhydrazone, and 1 μmol/L rotenone
500 and antimycin A for human hPAECs were added (XF Cell Mito Stress Test Kit, Agilent) through the
501 instrument's injection ports to obtain proton leak, maximal respiratory capacity, and nonmitochondrial
502 respiration, respectively. Glycolytic capacity was measured using an XF Glycolysis Stress Test Kit
503 (Seahorse Bioscience). ECAR was determined after serial injection with 10 mmol/L D-glucose, 1
504 μmol/L oligomycin, and 100 mmol/L 2-deoxyglucose. All the assays were performed in triplicate and
505 normalized to protein content.

506 **Endothelial Barrier Function**

507 TEER served as an indicator of barrier function of endothelial cell monolayers. TEER was
508 determined using an electrical cell-substrate impedance sensor (ECIS) (Applied Biophysics, Troy, NY,
509 USA). Briefly, the endothelial cells are seeded in complete medium into (8W10E -PET arrays Applied
510 Biophysics, NY, USA) each well and allowed them to grow until they reached confluence. The FFA
511 (0.25 mM, a combination of FFA 18:1, FFA 16:0 and FFA 18:0 (2:1:1)) was applied for 24 hours before
512 the barrier disruption was initiated by addition of recombinant human thrombin.

513 **Proliferation**

514 To investigate the proliferative effect of FFA treatment on hPASMCs, the following protocol
515 was applied (Biasin et al., 2014): 10 000 hPASMCs were seeded in 96-well plates; the following day
516 the cells were starved (VascuLife® Basal Medium, 0% FCS, 0.2% antibiotic/antimycotic) or kept under
517 control conditions (VascuLife® Basal Medium with 5% FCS; LifeLine Technology, Walkersville) for
518 12 h. Afterwards, platelet-derived growth factor (PDGF)-BB was added and the proliferation of
519 hPASMCs was determined by [^{3}H] thymidine (BIOTREND Chemikalien GmbH) incorporation, after
520 24 h of incubation, as an index of DNA synthesis and measured as radioactivity by scintillation counting
521 (Wallac 1450 MicroBeta TriLux Liquid Scintillation Counter and Luminometer). To investigate the
522 effect of FFA (0.25 mM, a combination of oleate, FFA 16:0 and FFA 18:0 (2:1:1)) on hPASMCs, the
523 same number of cells was seeded and after 12 h of starvation, FFA and vehicle were added and the
524 proliferation of hPASMCs was determined as aforementioned. All experiments were performed in
525 quadruplicate.

526 **DAF-DM-mediated nitric oxide measurement**

527 Measurements were performed as previously described[43]. hPAECs were seeded in gelatin-
528 coated dark 96-well plates, starved for 2 h with Ringer's solution and loaded with 10 µm 4-Amino-5-
529 Methylamino-2′,7′-Difluorofluorescein Diacetate (DAF-FM) for 30 min at 37°C. The cells were
530 stimulated with 5 µM acetylcholine (ACh) for the induction of nitric oxide measurement on
531 CLARIOstar Plus (BMG Labtech, Ortenberg, Germany) at Ex/Em = 495/515 nm. All the assays were
532 performed in quadruplicate and normalized to protein content.

533 **Plasma liquid chromatography–mass spectrometry metabolomics**

534 Metabolites were analysed by targeted hydrophilic interaction liquid chromatography–high
535 resolution mass spectrometry (HILIC-HRMS) metabolomics according to Bajad et al.[46] as described
536 previously[47,48]. Samples were processed according to Yuan et al.[49].

537 Samples from Graz were aliquoted and stored at the Biobank Graz. On the day of the processing
538 they were thawed in water ice bath on a slow rotary shaker (300 rpm) in < 10 min and vortexed shortly.

539 Aliquots of 100 µl were precipitated in LoBind Eppendorf tubes with 400 µl cold methanol (-80°C for
540 at least 4 h, kept on dry ice) and vortexed shortly. After the overnight precipitation at –80 °C the samples
541 were centrifuged for 10 min at 14.000 g at 4°C and supernatants transferred to fresh LoBind Eppendorf
542 tubes. Supernatants were dried under nitrogen flow and stored at –80°C until all batches of the cohort
543 were finished. Extracts were reconstituted in 100 µl 30% methanol/H_2O, vortexed for 45 s and
544 centrifuged for 5 min at 14.000 g at 4°C. The supernatant was transferred into autosampler vials, and
545 equal aliquots from all samples were pooled for quality control (QC). All ready-to-measure extracts
546 were refrozen at –80°C prior to measurement. Every 24 h samples were freshly thawed at RT, vortexed,
547 spun down and added to the autosampler at 4°C.

548 Measurements were made in independent runs per cohort with samples in randomized order,
549 interspaced by according blanks, pooled QC samples and UltimateMix (UM, mix described previously
550 (Vogel et al., 2019)). Pooled QC samples were generated independently for cohort 1 and 2, while QC
551 was mixed for cohort 3 and 4. Cohorts 1 and 2 were extracted and measured in 1 batch, while cohorts
552 3 and 4 were randomly divided into 6 batches for sample extraction and measured with daily thawed
553 extracts to reduce metabolite degradation.

554 Extracts were measured with a Dionex Ultimate 3000 high-performance liquid chromatography
555 (HPLC) setup (Thermo Fisher Scientific, USA) equipped with a NH_2-Luna HILIC analytical column
556 and crudcatcher with an injection volume of 10 µl and a 37 min gradient from aqueous acetonitrile
557 solution [(5% acetonitrile v/v), 20 mM ammonium acetate, 20 mM ammonium hydroxide, pH 9.45] as
558 eluent A (LMA) to acetonitrile as eluent B (LMB). Mass spectrometric detection was carried out with
559 a Q-Exactive™ system (Thermo Fisher Scientific). Electrospray ionization (ESI) was used for negative
560 and positive ionization and masses between 70 and 1050 m/z were detected.

561 Raw data were converted to mzXML using msConvert (ProteoWizard Toolkit v3.0.5), and
562 target metabolites were extracted using the in-house developed tool PeakScout. Spectrum slices were
563 presented around the exact target mass (± 50 ppm) and retention time (± 3 min) in accordance with the
564 standards described by Sumner et al.[50]. For each target metabolite all peak area integrations were
565 manually confirmed in each sample. Molecular masses of target metabolites were taken from literature
566 and available online databases (HMDB, KEGG, Metlin)[51–53]. In addition, pure substances of all
567 hydrophilic metabolites and selected lipophilic metabolites were run on the same system to obtain
568 accurate reference retention times and fragmentation spectra.

569 The analytical quality of all targeted metabolites was strictly graded to be suitable for
570 multivariate analysis and univariate analysis using the following parameters: deviation from target mass
571 < 5 ppm, mass difference range < 10 ppm, retention time standard deviation < 0.75 min, percentage of
572 missing values < 30%, relative standard deviation in QC after drift correction <30%, and blank load in
573 QC < 30%. Of 164 included metabolites, 11 metabolites were considered unsuitable for ROC analysis

574 due to lower signal intensity and lower consistency in repeated sample measurements (controls in
575 cohorts 3 and 4).

576 Analytical quality of samples, blanks, QC, and UM was graded by sample median, peak shapes,
577 retention time shifts, percentage of missing values < 30%, and position in the PCA scores plot. From
578 cohort 2, the first two UM and from cohort 4 the last four QC did not meet the quality criteria and were
579 therefore excluded.

580 **Statistical analysis**

581 Data visualisation and statistical analysis were performed with R v4.0.2 (R Core Team, 2020)
582 (using the packages readxl, openxlsx, stringr, dplyr, tidyr, doParallel, statTarget, car, colorspace,
583 RColorBrewer, ggplot2, ggforce, ggpmisc, ggpubr, scales, grid, ellipse, correlation, dendsort,
584 pheatmap, nlme, emmeans, missMDA, FactoMineR, mixOmics, MetaboAnalystR 3.0.3, survival,
585 survminer, pROC, caret, patchwork) and TIBCO Spotfire v11.8.0, TIBCO, Palo Alto, CA. Graphpad
586 Prism v9 has been used to assess differences in the *in vitro* experiments.

587 Typically, MS results are relative and only comparable within the same run. However, recent
588 advances in drift correction allow to merge data for joint analysis. Peak areas without drift correction
589 were log_{10}-transformed prior to all further analysis. The drift correction was based on the RF driven
590 algorithm that used QC measurements to model batch effects and drift for each metabolite with
591 *statTarget::shiftCor(., Frule = 0.7, ntree = 500, impute = "KNN", coCV = 100, QCspan = 0, degree*
592 *= 2)* [54]. The imputed, drift-corrected data were multiplied by 10^3 to make the numbers more readable
593 after log_{10}-transformation. In the drift corrected, log_{10}-transformed data all imputed values were
594 removed and data was trimmed by median absolute deviation (MAD) score[55], assuming a normal
595 distribution (multiplication with 1.4826). Strong single outliers were removed with a very conservative
596 threshold of having an absolute MAD score > 4 (165 single values in 65 metabolites). Data for all
597 metabolites and samples is provided in Supplementary Data 1 with and without drift correction.

598 In order to ensure validity of drift correction and subsequent results, each measurement run was
599 first analysed independently with unsupervised multivariate (iPCA), supervised multivariate (OPLS-
600 DA) and univariate on log_{10}-transformed data without drift correction (see Fig. S1). Next, drift
601 corrected, log_{10}-transformed data from all runs was jointly analysed with the same methods. The drift
602 correction successfully removed the significant difference between measurement runs and notably
603 reduced the technical variability in all metabolites (Fig. S2). Additionally, no difference was observed
604 based on center or sample material type (Fig. S2). Replicate measurements of samples in different runs
605 were average on drift corrected data to yield one metabolome per patient for subsequent analysis one
606 metabolome per patient.

607 All reported p-values were adjusted for multiple testing according to Benjamini–Hochberg
608 (BH) denoted as p_{BH} (*stats::p.adjust()*)[56]. Distribution and scedasticity were investigated with
609 Kolmogorov–Smirnov test (*stats::ks.test()*) and Brown–Forsythe Levene-type test (*car::leveneTest()*)
610 [57], respectively. After log_{10}-transformation data was mostly normally distributed with 91% of all
611 metabolites without drift correction and 99% of all metabolites with drift correction testing not
612 significant ($p_{BH} > 0.05$). Analog, data was mostly homoscedastic with 79% without drift correction and
613 80% with drift correction of all metabolites testing not significant ($p_{BH} > 0.05$).

614 For iPCA missing values were imputed with *missMDA::imputePCA(., ncp = 10)*[58] and analysis
615 was performed scaled and centred to unit variance (z-scaled) with *mixOmics::ipca(., scale = TRUE,*
616 *ncomp = 2, mode = "deflation")*[59].

617 For OPLS-DA missing values were imputed with *MetaboAnalystR::ImputeMissingVar(.,*
618 *method = "knn_var")*[60], data was scaled and centred to unit variance (z-scaled) with
619 *MetaboAnalystR::Normalization(..., "AutoNorm")* and models were calculated with
620 *MetaboAnalystR::OPLSR.Anal(., reg = TRUE)* with a standard 7-fold cross-validation for the factor
621 *disease*. Model stability was additionally verified with 1000 random label permutations by
622 *MetaboAnalystR::OPLSDA.Permut(., num = 1000)*.

623 Pearson correlation were calculated for each metabolite (drift corrected, log_{10}-transformed data)
624 against each numeric clinical parameter (untransformed) with *correlation::correlation()*[61]. Results were
625 filtered to retain only metabolites and clinical parameters with at least one significant correlation
626 ($p_{BH} < 0.05$). Retained correlations were clustered by Lance-Williams dissimilarity update with
627 complete linkage using *stats::dist()* and *stats::hclust()*. Dendogram were sorted with
628 *dendsort::dendsort()*[62] at every merging point according to the average distance of subtrees and plotted
629 at the corresponding heat maps of Pearson R with *pheatmap::pheatmap()*[63].

630 For univariate analysis of significant changes within each metabolite for the factor *disease* (i.e.
631 PH vs. HC/DC) generalized least squares models were fitted with *nlme::gls()*[64,65] without confounders
632 and with potential confounders (age, sex, BMI) by maximum likelihood. For analysis within each cohort
633 log_{10}-transformed data was used, for joint analysis over all cohorts drift corrected, log_{10}-transformed
634 data was used, thus constituting a nonlinear approach. The three most common potential confounders
635 (age, sex, BMI) were added stepwise in all possible combinations and model performances were
636 compared within each metabolite by lower AIC (Akaike information criterion; relative estimate of
637 information loss), higher log-likelihood (goodness of fit), significance in log-likelihood ratio test
638 comparing two models, quality of Q-Q plots, randomness in residual and direct comparison of t-ratios.
639 All models with any confounder combination showed significant influence ($p < 0.01$) on selected few
640 metabolites (13–39). The model with age + sex impacted most metabolites. However, a direct

comparison of t-ratio revealed a very small impact of age or sex correction on results, and according to model parsimony models without confounders were reported throughout.

FFA/lipid-ratios were calculated with FFAs in the numerator and lipids in the denominator. The numerators were all possible, summed (not weighed) combinations of up to six FFA from 11 FFAs (most significant in univariate analysis PH versus HC/DC and best analytical quality): FFA C15:0, FFA C16:2, FFA C16:1, FFA C17:1, FFA C17:0, FFA C18:3, FFA C18:2, FFA C18:1, FFA C19:1, FFA C20:5 and FFA C20:1. The denominators were all possible, summed (not weighed) combinations of up to four lipids from eight lipids (no significant change in univariate analysis and best analytical quality): LPC 18:2, LPC 18:1, PC 36:4, PC 38:6, SM 34:2, SM 36:2, LPE 16:0, and LPE 18:1. The combination of all possible summed FFA numerator and summed lipid denominator yielded a total of 246 842 different FFA/lipid-ratios. All used FFA and lipids had no missing values. The technical variability RSD in QC was calculated for each FFA/lipid-ratio following the rules of error propagation from the single metabolites RSD of QC in drift corrected, log_{10}-transformed data. All FFA/lipid-ratios were calculated once without and once with drift correction (both log_{10}-transformed). Diagnostic performance was tested by ROC analysis with *pROC::roc(..., algorithm = 2)*[66] based on our training cohort. Test data like in machine learning approaches was not needed here because ratios are directly calculated without any model training. Therefore logistic regression was performed fitting training data with *stats::glm(..., family = "binomial").* The performance was evaluated on the validation cohort using *pROC::roc()*. The optimal threshold was determined with *pROC::coords(..., ,best.method = "closest.topleft")* to determine sensitivity and specificity.

Survival analysis used either times since sampling or times since diagnosis defining confirmed death as endpoint while censoring all others at time of last known follow-up. Impact of all relevant clinical parameters (untransformed), all single metabolites (drift corrected, log_{10}-transformed data) and best performing FFA/lipid-ratios (log_{10}-transformed data without drift correction) was analysed. FPHR4p scores were inverted so that higher values represent higher mortality risk. Numerical parameters were split into *high* and *low* with maxstat as optimal cut-off for survival prediction as determined by *survminer::surv_cutpoint(..., minprop = 0.3)*[67]. Kaplan–Meier curves were fitted for each category with *survival::survfit()*[68], differences were tested with *survminer::ggsurvplot()* and plots with time since diagnosis were truncated at 15 years for better comparability with times since baseline (i.e. time since sampling). The Cox HR analysis[69] was calculated with *survminer::coxph()* for the confounders (age, sex, BMI), the COMPERA 2.0 score, FPHR4p, and RATIO1 alone or in combinations. Numeric factors were categorized into *high* and *low* same as for Kaplan-Meier curves. The combination of RATIO1 with the FPHR4p or COMPERA 2.0 score was done additively with the same weighting on scaled values from 0 to 1, rescaling after addition.

Data visualisation and calculation of the machine learning and Cox HR analysis was performed with Python 3.9 (using the packages pandas, numpy, seaborn, sklearn, matplotlib, xgboost)[70–73].

For machine learning, the package sklearn[74] was used for the random forest (RF) and package xgboost for the XGBoost[19] implementation. Data was normalized with mean 0 and variance 1. A hyperparameter search for *number of trees {101, 301, 1001, 2001,* ***3001****}* and *depth {5, 10, 100, 200,* ***300****}* for RF and *eta {0.1,* ***0.01****, 0.001}*, *depth {****5****, 10, 100, 200, 300}* and *n_estimators {101, 301, 1001, 2001,* ***3001****}* for XGBoost was conducted with finally used hyperparameters highlighted in bold. Models were trained on trainings data with five random splits (stratified by group, age, sex) into 80% training data tested against the remainder 20% data from the split. Models were validated with the external validation cohort.

Language editing was aided by the artificial intelligence tool https://instatext.io/ (accessed February 2023).

Supplemental Information

Supplemental Information can be found attached to this publication.

Materials Availability

This study did not generate new unique reagents.

Data and Code Availability

The author declare that all data supporting the findings in this study are available in the online supplementary data 1 and online repositories. Mass spectrometric data have been deposited in https://zenodo.org under doi: 10.5281/zenodo.7857706. Data is provided de-identified and is available immediately after publication with no end for those who wish to access the data for any purpose. The provided *Sample_Name* in the online supplementary data 1 links to the file names in the online repository and are unsuitable to identify single patients. The primary key is only known to part of the study team. Due to the sensitive nature of potentially identifying information exact age can only be provided upon reasonable request

Author contributions

Conceptualisation, NB, BMN, TP, HO, AO; Data curation, NB, BMN, EZ, HL, UB, HO, AO; Formal analysis, NB, BMN, EZ, HL, UB, HO, AO; Funding acquisition, NB, TP, HO, AO; Investigation, NB, BMN, EZ, VF, CN, VB, HO, AO; Methodology, NB, BMN, EZ, CN, AO, HO; Project administration, NB, BMN, UB, VF, KH, SU, TJL, HO, AO; Resources, NB, BN, EZ, CM, HL, UB, KH; SU, TJL, TP, HO, AO; Software, NB, HL; Supervision, NB, EZ, UB, HO, AO; Validation,

NB, BN, EZ, HL, VF, CN, VB, SU, TJL, HO, AO; Visualisation, NB, BMN, HL, CN, VB, AO; Writing – original draft, NB, BAM, HO, AO; Writing – Review & Editing, all authors;

Acknowledgements

We are very grateful for the excellent technical assistance from Elisabeth Blanz, Sabine Halsegger, Daniela Kleinschek, Jessica Schweiger, Yasemin Gassner, Gert Trausinger and Edgar Gander. We express our heartfelt gratitude to Saskia Trescher, Pablo López-García, Sophie Narath, Michael Pienn and Peter Wolf for their valuable discussions and helpful advices.

Funding

NB, TP disclose that part of this work has been carried out with the K1 COMET Competence Center CBmed, which is funded by the Federal Ministry of Transport, Innovation and Technology; the Federal Ministry of Science, Research and Economy; Land Steiermark (Department 12, Business and Innovation); the Styrian Business Promotion Agency; and the Vienna Business Agency. The COMET program is executed by the Österreichische Forschungsförderungs GmbH FFG. VB is supported by the Austrian Science Foundation (FWF, T1032-B34).

Competing interests

Several authors (NB, CM, AO, BMN, HO) are inventors of the patent "*Biomarker for the diagnosis of pulmonary hypertension (PH)*" WO2017153472A1 (priority date 09.03.2016, granted in US, KR, JP, pending in CA, EP, AU) being jointly held by CBmed Gmbh, Joanneum Research Forschungsgesellschaft mbH, Medical University Graz and Ludwig Boltzmann Gesellschaft GmbH. The authors received no personal financial gain from the patent.

During work on this publication NB was partially employed at CBmed GmbH. TP is chief scientific officer (CSO) of CBmed GmbH. EZ and CM were employed at Joanneum Research Forschungsgesellschaft mbH. The employing companies provided support in the form of salaries, materials and reagents but did not have any additional role in the study design, data collection and analysis, decision to publish, or preparation of the manuscript.

VF received honoraria for lectures, presentations, speakers bureaus, manuscript writing, or educational events from Janssen, Chiesi, BMS, and Boehringer Ingelheim and support for attending meetings, and/or travel from Janssen, MSD, and Boehringer Ingelheim outside the submitted work.

CN received support for attending meetings, and/or travel from Boehringer Ingelheim and Inventiva pharma outside the submitted work.

BAM reports personal fees from Actelion Pharmaceuticals, Tenax and Regeneron, grants from Deerfield Company, NIH (5R01HL139613-03, R01HL163960, R01HL153502, R01HL155096-01), Boston Biomedical Innovation Ceter (BBIC), Brigham IGNITE award, Cardiovascular Medical

research Education Foundation outside the submitted work. BAM reports patent PCT/US2019/059890 (pending), PCT/US2020/066886 (pending) and #9,605,047 (granted) not licensed and outside the submitted work.

SU received grants from the Swiss National Science Foundation, Zürich and Swiss Lung League, EMDO-Foundation, Orpha-Swiss, Janssen and MSD all unrelated to the present work. SU received consultancy fees and travel support from Orpha-Swiss, Janssen, MSD and Novartis unrelated to the present work.

TJL reports grants for his institution from Acceleron Pharma, Gossamer Bio, Janssen-Cilag, and United Therapeutics; personal fees and non-financial support from Acceleron Pharma, AstraZeneca, Boehringer Ingelheim, Gossamer Bio, Ferrer, Janssen-Cilag, MSD, Orphacare, and Pfizer outside the submitted work.

KH is a consultant at Medtronic Österreich GmbH outside the submitted work.

TP reports grants from AstraZeneca, Novo Nordisk, Sanofi paid to the Medical University of Graz outside the submitted work. TP reports personal fees and nonfinancial support from Novo Nordisk and Roche Diagnostics outside the submitted work.

HO reports grants from Bayer, Unither, Actelion, Roche, Boehringer Ingelheim, and Pfizer. HO reports personal fees and nonfinancial support from Medupdate and Mondial, AOP, Bayer, Actelion, Pfizer, Ferrer, Novartis, Astra Zeneca, Boehringer Ingelheim, Chiesi, Menarini, MSD, and GSK outside the submitted work.

AO received honoraria for presentations and support for attending meetings, and/or travel from MSD outside the submitted work.

No conflict of interest, financial or otherwise, are declared by the authors HL and UB.

References

1. Humbert, M. *et al.* 2022 ESC/ERS Guidelines for the diagnosis and treatment of pulmonary hypertension. *Eur Respir J* **61**, (2023).
2. Hoeper, M. M. *et al.* A global view of pulmonary hypertension. *Lancet Respir Med* **4**, 306–322 (2016).
3. Vachiéry, J.-L. *et al.* Pulmonary hypertension due to left heart disease. *Eur Respir J* **53**, (2019).
4. Nathan, S. D. *et al.* Pulmonary hypertension in chronic lung disease and hypoxia. *Eur Respir J* **53**, (2019).
5. Maron, B. A. *et al.* Pulmonary vascular resistance and clinical outcomes in patients with pulmonary hypertension: a retrospective cohort study. *Lancet Respir Med* **8**, 873–884 (2020).
6. Douschan, P. *et al.* Mild Elevation of Pulmonary Arterial Pressure as a Predictor of Mortality. *Am J Respir Crit Care Med* **197**, 509–516 (2018).
7. Farber, H. W. *et al.* Five-Year outcomes of patients enrolled in the REVEAL Registry. *Chest* **148**, 1043–54 (2015).
8. Zelt, J. G. E. *et al.* Mortality trends in pulmonary arterial hypertension in Canada: a temporal analysis of survival per ESC/ERS guideline era. *Eur Respir J* **59**, (2022).
9. Kräuter, C. *et al.* Automated vortical blood flow-based estimation of mean pulmonary arterial pressure from 4D flow MRI. *Magn Reson Imaging* **88**, 132–141 (2022).
10. Brittain, E. L. *et al.* Fatty acid metabolic defects and right ventricular lipotoxicity in human pulmonary arterial hypertension. *Circulation* **133**, 1936–1944 (2016).
11. Hemnes, A. R. *et al.* Human PAH is characterized by a pattern of lipid-related insulin resistance. *JCI Insight* **4**, (2019).
12. Lewis, G. D. *et al.* Metabolic Profiling of Right Ventricular-Pulmonary Vascular Function Reveals Circulating Biomarkers of Pulmonary Hypertension. *J Am Coll Cardiol* **67**, 174–189 (2016).
13. Rhodes, C. J. *et al.* Plasma Metabolomics Implicates Modified Transfer RNAs and Altered Bioenergetics in the Outcomes of Pulmonary Arterial Hypertension. *Circulation* **135**, 460–475 (2017).
14. Nagy, B. M. *et al.* Importance of kynurenine in pulmonary hypertension. *American Journal of Physiology-Lung Cellular and Molecular Physiology* **313**, L741–L751 (2017).
15. Nagy, B. M. *et al.* No indication of insulin resistance in idiopathic PAH with preserved physical activity. *European Respiratory Journal* vol. 55 Preprint at https://doi.org/10.1183/13993003.01228-2019 (2020).
16. Wertheim, B. M. *et al.* Proline and glucose metabolic reprogramming supports vascular endothelial and medial biomass in pulmonary arterial hypertension. *JCI Insight* **8**, (2023).
17. Breiman, L. Random forests. *Mach Learn* **45**, 5–32 (2001).
18. Breiman, L., Friedman, J. H. (Jerome H.), Olshen, R. A. & Stone, C. J. *Classification and regression trees*. (1984).
19. Chen, T. & Guestrin, C. XGBoost. in *Proceedings of the 22nd ACM SIGKDD International Conference on Knowledge Discovery and Data Mining* 785–794 (ACM, 2016). doi:10.1145/2939672.2939785.
20. Boucly, A. *et al.* Risk assessment, prognosis and guideline implementation in pulmonary arterial hypertension. *European Respiratory Journal* **50**, (2017).
21. Hoeper, M. M. *et al.* COMPERA 2.0: a refined four-stratum risk assessment model for pulmonary arterial hypertension. *European Respiratory Journal* **60**, (2022).
22. Bourgin, M. *et al.* Circulating acetylated polyamines correlate with Covid-19 severity in cancer patients. *Aging* **13**, 20860–20885 (2021).
23. Kibe, R. *et al.* Upregulation of colonic luminal polyamines produced by intestinal microbiota delays senescence in mice. *Sci Rep* **4**, 4548 (2015).
24. Willeit, P. *et al.* Asymmetric dimethylarginine and cardiovascular risk: Systematic review and meta-analysis of 22 prospective studies. *J Am Heart Assoc* **4**, (2015).
25. Delcroix, M. & Howard, L. Pulmonary arterial hypertension: the burden of disease and impact on quality of life. *European Respiratory Review* **24**, 621–629 (2015).
26. Kovacs, G. *et al.* An official European Respiratory Society statement: pulmonary haemodynamics during exercise. *European Respiratory Journal* **50**, 1700578 (2017).
27. Paulin, R. & Michelakis, E. D. The Metabolic Theory of Pulmonary Arterial Hypertension. *Circ Res* **115**, 148–164 (2014).
28. Talati, M. H. *et al.* Mechanisms of Lipid Accumulation in the Bone Morphogenetic Protein Receptor Type 2 Mutant Right Ventricle. *Am J Respir Crit Care Med* **194**, 719–28 (2016).
29. Hemnes, A. R. *et al.* Evidence for right ventricular lipotoxicity in heritable pulmonary arterial hypertension. *Am J Respir Crit Care Med* **189**, 325–34 (2014).
30. Harbaum, L. *et al.* Mining the Plasma Proteome for Insights into the Molecular Pathology of Pulmonary Arterial Hypertension. *Am J Respir Crit Care Med* **205**, 1449–1460 (2022).
31. Rhodes, C. J. *et al.* Using the Plasma Proteome for Risk Stratifying Patients with Pulmonary Arterial Hypertension. *Am J Respir Crit Care Med* **205**, 1102–1111 (2022).

32. Bhatt-Wessel, B., Jordan, T. W., Miller, J. H. & Peng, L. Role of DGAT enzymes in triacylglycerol metabolism. *Arch Biochem Biophys* **655**, 1–11 (2018).
33. Chambers, K. T. *et al.* Myocardial Lipin 1 knockout in mice approximates cardiac effects of human LPIN1 mutations. *JCI Insight* **6**, (2021).
34. Reue, K. The lipin family: mutations and metabolism. *Curr Opin Lipidol* **20**, 165–70 (2009).
35. Takeuchi, K. & Reue, K. Biochemistry, physiology, and genetics of GPAT, AGPAT, and lipin enzymes in triglyceride synthesis. *Am J Physiol Endocrinol Metab* **296**, E1195-209 (2009).
36. Kovacs, G. *et al.* Changes in pulmonary exercise haemodynamics in scleroderma: a 4-year prospective study. *Eur Respir J* **50**, (2017).
37. Kovacs, G. *et al.* Severe Pulmonary Hypertension in COPD: Impact on Survival and Diagnostic Approach. *Chest* **162**, 202–212 (2022).
38. Haudum, C. W. *et al.* Cohort profile: 'Biomarkers of Personalised Medicine' (BioPersMed): a single-centre prospective observational cohort study in Graz/Austria to evaluate novel biomarkers in cardiovascular and metabolic diseases. *BMJ Open* **12**, e058890 (2022).
39. Galiè, N. *et al.* 2015 ESC/ERS Guidelines for the diagnosis and treatment of pulmonary hypertension: The Joint Task Force for the Diagnosis and Treatment of Pulmonary Hypertension of the European Society of Cardiology (ESC) and the European Respiratory Society (ERS): Endorsed by: Association for European Paediatric and Congenital Cardiology (AEPC), International Society for Heart and Lung Transplantation (ISHLT). *Eur Respir J* **46**, 903–75 (2015).
40. Hoffmann, J. *et al.* Distinct differences in gene expression patterns in pulmonary arteries of patients with chronic obstructive pulmonary disease and idiopathic pulmonary fibrosis with pulmonary hypertension. *Am J Respir Crit Care Med* **190**, 98–111 (2014).
41. Nagaraj, C. *et al.* Hypoxic vascular response and ventilation/perfusion matching in end-stage COPD may depend on p22phox. *Eur Respir J* **50**, (2017).
42. Papp, R. *et al.* Targeting TMEM16A to reverse vasoconstriction and remodelling in idiopathic pulmonary arterial hypertension. *Eur Respir J* **53**, (2019).
43. Skofic Maurer, D. *et al.* Endothelial Dysfunction Following Enhanced TMEM16A Activity in Human Pulmonary Arteries. *Cells* **9**, (2020).
44. Stulnig, G. *et al.* Docosahexaenoic acid (DHA)-induced heme oxygenase-1 attenuates cytotoxic effects of DHA in vascular smooth muscle cells. *Atherosclerosis* **230**, 406–413 (2013).
45. Kikuchi, N. *et al.* Selenoprotein P Promotes the Development of Pulmonary Arterial Hypertension: Possible Novel Therapeutic Target. *Circulation* **138**, 600–623 (2018).
46. Bajad, S. U. *et al.* Separation and quantitation of water soluble cellular metabolites by hydrophilic interaction chromatography-tandem mass spectrometry. *J Chromatogr A* **1125**, 76–88 (2006).
47. Fröhlich, E. E. *et al.* Cognitive impairment by antibiotic-induced gut dysbiosis: Analysis of gut microbiota-brain communication. *Brain Behav Immun* **56**, 140–155 (2016).
48. Mueller, K. M. *et al.* Adipocyte Glucocorticoid Receptor Deficiency Attenuates Aging- and Hfd-Induced Obesity, and Impairs the Feeding-Fasting Transition. *Diabetes* **66**, 272–286 (2017).
49. Yuan, M., Breitkopf, S. B., Yang, X. & Asara, J. M. A positive/negative ion-switching, targeted mass spectrometry-based metabolomics platform for bodily fluids, cells, and fresh and fixed tissue. *Nat Protoc* **7**, 872–81 (2012).
50. Sumner, L. W. *et al.* Proposed minimum reporting standards for chemical analysis Chemical Analysis Working Group (CAWG) Metabolomics Standards Initiative (MSI). *Metabolomics* **3**, 211–221 (2007).
51. Guijas, C. *et al.* METLIN: A Technology Platform for Identifying Knowns and Unknowns. *Anal Chem* **90**, 3156 (2018).
52. Kanehisa, M., Sato, Y., Kawashima, M., Furumichi, M. & Tanabe, M. KEGG as a reference resource for gene and protein annotation. *Nucleic Acids Res* **44**, D457–D462 (2016).
53. Wishart, D. S. *et al.* HMDB 4.0: The human metabolome database for 2018. *Nucleic Acids Res* **46**, D608–D617 (2018).
54. Luan, H., Ji, F., Chen, Y. & Cai, Z. statTarget: A streamlined tool for signal drift correction and interpretations of quantitative mass spectrometry-based omics data. *Anal Chim Acta* **1036**, 66–72 (2018).
55. Leys, C., Ley, C., Klein, O., Bernard, P. & Licata, L. Journal of Experimental Social Psychology Detecting outliers : Do not use standard deviation around the mean, use absolute deviation around the median. *Experimental Social Psychology* 4–6 (2013).
56. Benjamini, Y. & Hochberg, Y. Controlling the False Discovery Rate: A Practical and Powerful Approach to Multiple Testing. *Journal of the Royal Statistical Society: Series B (Methodological)* **57**, 289–300 (1995).
57. Brown, M. B. & Forsythe, A. B. Robust Tests for the Equality of Variances. *J Am Stat Assoc* **69**, 364 (1974).

58. Husson, F. & Josse, J. missMDA: Handling Missing Values with Multivariate Data Analysis. *R package version 1.8.2.* Preprint at http://cran.r-project.org/package=missMDA (2015).
59. Rohart, F., Gautier, B., Singh, A. & Lê Cao, K.-A. mixOmics: An R package for 'omics feature selection and multiple data integration. *PLoS Comput Biol* **13**, e1005752 (2017).
60. Pang, Z., Chong, J., Li, S. & Xia, J. MetaboAnalystR 3.0: Toward an Optimized Workflow for Global Metabolomics. *Metabolites* **10**, 186 (2020).
61. Makowski, D., Ben-Shachar, M., Patil, I. & Lüdecke, D. Methods and Algorithms for Correlation Analysis in R. *J Open Source Softw* **5**, 2306 (2020).
62. Sakai, R. & Biederstedt, E. dendsort: modular leaf ordering methods for dendrogram representations in R. Preprint at https://doi.org/10.12688/f1000research.4784.1 (2021).
63. Kolde, R. pheatmap: Pretty Heatmaps. *R package version 1.0.12* Preprint at https://CRAN.R-project.org/package=pheatmap (2019).
64. Pinheiro, J., Bates, D. & R Core Team. nlme: Linear and Nonlinear Mixed Effects Models. Preprint at https://CRAN.R-project.org/package=nlme (2022).
65. Pinheiro, J., Bates, D., DebRoy, S., Sarkar, D. & R Core Team. nlme: Linear and Nonlinear Mixed Effects Models. *R package version 3.1-122* vol. 3 57 Preprint at http://cran.r-project.org/package=nlme (2015).
66. Robin, X. *et al.* pROC: An open-source package for R and S+ to analyze and compare ROC curves. *BMC Bioinformatics* **12**, 77 (2011).
67. Kassambara, A., Kosinski, M. & Biecek, P. survminer: Drawing Survival Curves using 'ggplot2'. Preprint at https://CRAN.R-project.org/package=survminer (2021).
68. Therneau, T. M. Package for Survival Analysis in R. Preprint at https://CRAN.R-project.org/package=survival (2021).
69. Cox, D. R. Regression Models and Life-Tables. *Journal of the Royal Statistical Society: Series B (Methodological)* **34**, 187–202 (1972).
70. Harris, C. R. *et al.* Array programming with NumPy. *Nature* **585**, 357–362 (2020).
71. McKinney, W. Data Structures for Statistical Computing in Python. in *PROC. OF THE 9th PYTHON IN SCIENCE CONF. (SCIPY 2010)* 56–61 (2010).
72. Waskom, M. *et al.* mwaskom/seaborn: v0.8.1 (September 2017). Preprint at https://doi.org/10.5281/zenodo.883859 (2017).
73. Hunter, J. D. Matplotlib: A 2D Graphics Environment. *Comput Sci Eng* **9**, 90–95 (2007).
74. Pedregosa, F. *et al.* Scikit-learn: Machine Learning in Python. *Journal of Machine Learning Research* **12**, 2825–2830 (2011).

Supplementary Figures

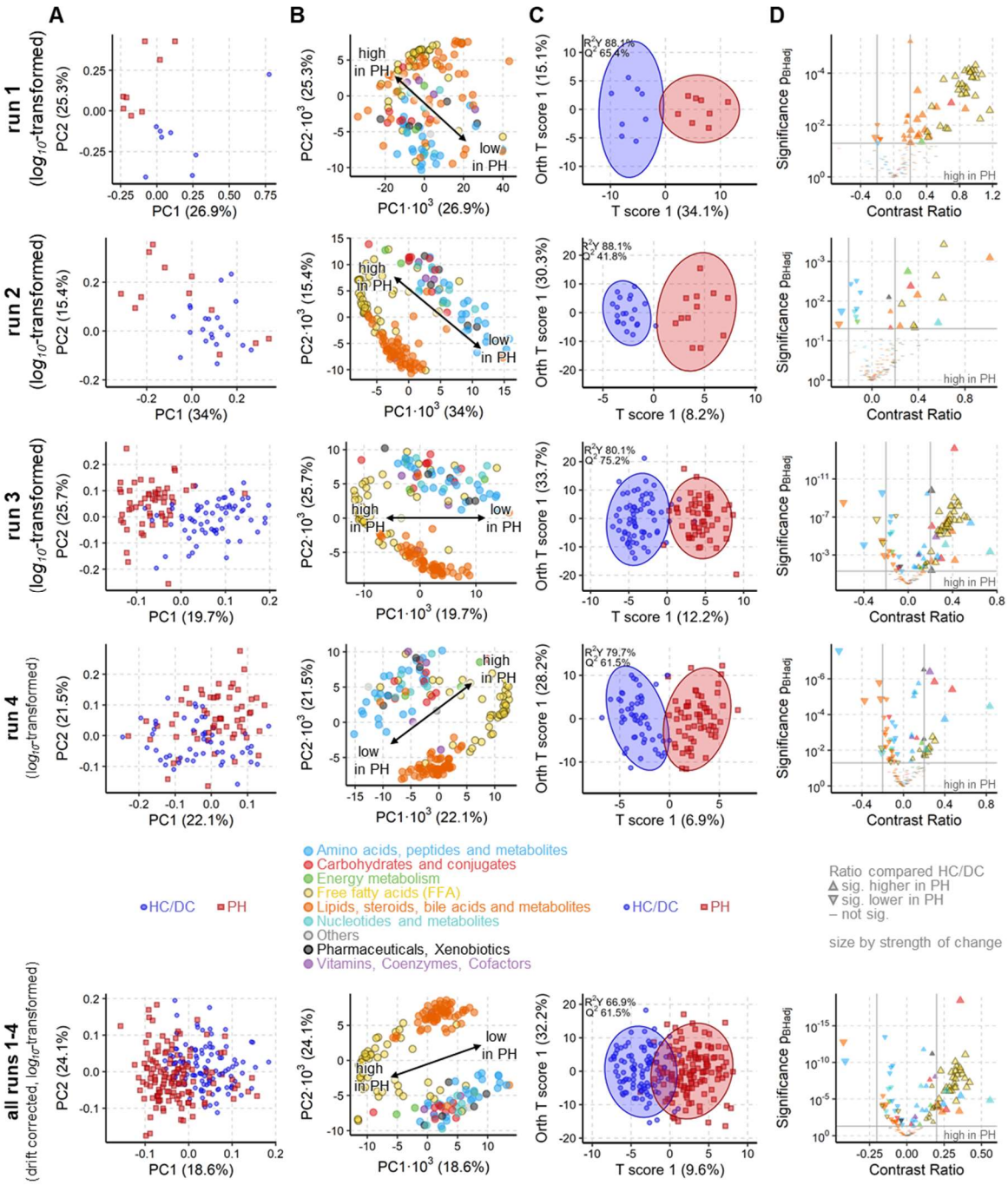

Fig. S1. PH is associated with a strong metabolic shift in every measurement run. (A) iPCA scores plot representing the metabolic profile of each sample as a dot. The proximity of the dots indicates the similarity of the subjects' metabolomes. Clear group separation by PH is visible along the first and or second component for each run and when all runs are jointly analyzed. **(B)** To A corresponding loadings plot in which each dot represents the contribution of the metabolite to the group separation observed in the scores plot. Free fatty acids (FFA, yellow circles) strongly drive the group separation and are increased in PH patients. **(C)** OPLS-DA maximizes the group difference from PH to HC/DC and the resulting scores plot represents, as in A, with dots the metabolome of each subjects. Similarly, proximity indicates similarity and ellipses mark the 95% confidence interval of the groups. The

difference between the metabolome of PH and HC/DC was significant ($Q^2 > 50\%$, $p < 0.001$). **(D)** Volcano plot of univariate analysis highlighting significant ($p_{BH} < 0.05$, grey horizontal line) and strong (absolute contrast ratio > 0.25, grey vertical lines) increase in FFAs. For all methods 164 known metabolites and all samples from the measurement run per cohort ($n_1 = 16$, $n_2 = 33$, $n_3 = 118$, $n_4 = 109$) on log_{10}-transformed was used. In run 4 measurement all HC samples from run 3 were repeated to evaluate reproducibility of samples across measurement runs.

920

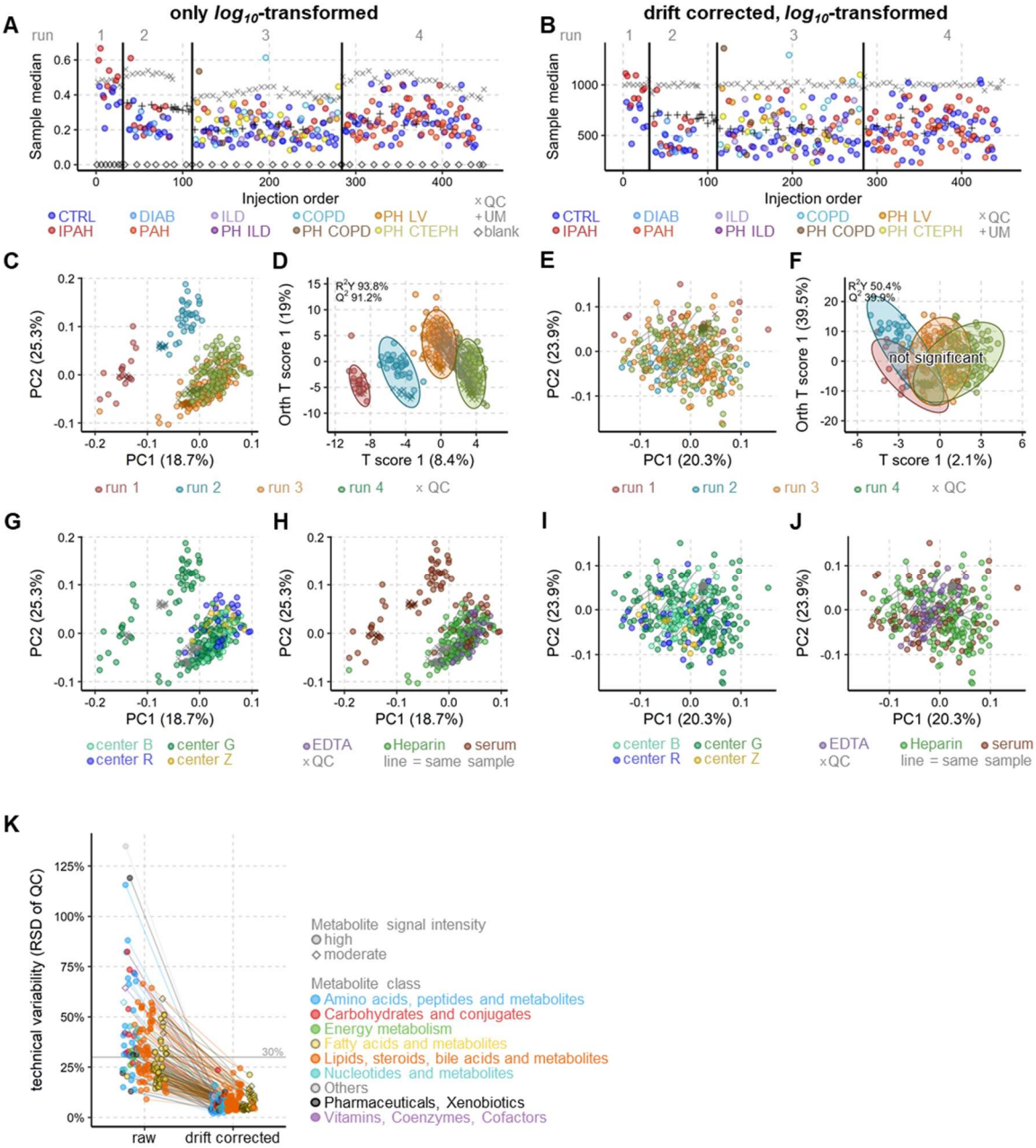

Fig. S2. Drift correction improves data quality enabling a unified analysis of all 4 measurement runs. (A, B) Plot of the sample's median signal intensity of all metabolites versus the sequence of measurement with measurements runs being separated by vertical black lines. **(A)** The QC samples (grey x) fluctuate within each measurement (= drift), while the batch effect is well visible as signal intensity jumps between the measurements. **(B)** Drift

correction with an RF-based algorithm on QC samples removed drift and batch effects from the median sample intensity. **(C, E, G, H, I, J)** iPCA scores plots plot representing the metabolic profile of each sample as a dot. The proximity of the dots indicates the similarity of the metabolomes. Lines connect replicate measurements from same samples. Note **(C, G, H)** are the same iPCA model highlighting different biological factors. Analog **(E, I, J)** are the same iPCA model. **(C)** A clear group separation by measurement run is well visible between all 4 runs, with runs 3 and 4 being more similar due to the back to back measurement and shared HC and QC samples. **(D)** Drift correction removes the separation by measurement run. (D, F) OPLS-DA maximizes the differences between runs 1 to 4 and the resulting scores plot represents, as in C, with dots the metabolome of each sample. Similarly, proximity indicates similarity and ellipses mark the 95% confidence interval of the groups. **(D)** All 4 measurement runs were highly significantly ($Q^2 > 50\%$, $p < 0.001$) different before drift correction and **(F)** become non-significant after drift correction. **(G, I)** The observed group separation by sample origin (study center) before drift correction was significantly reduced after drift correction. **(H, J)** The observed group separation by sample material type before drift correction was significantly reduced after drift correction. **(K)** The strong reduction of the technical variability over all 4 runs after drift corrections shows how well the RF-based algorithm reduced technical noise. All plots are based on 164 known metabolites and all samples from the measurement run per cohort ($n_1 = 16$, $n_2 = 33$, $n_3 = 118$, $n_4 = 109$). A, C, D, G, H used log_{10}-transformed. B, E, F, I, J used log_{10}-transformed, drift corrected data.

921

922

923

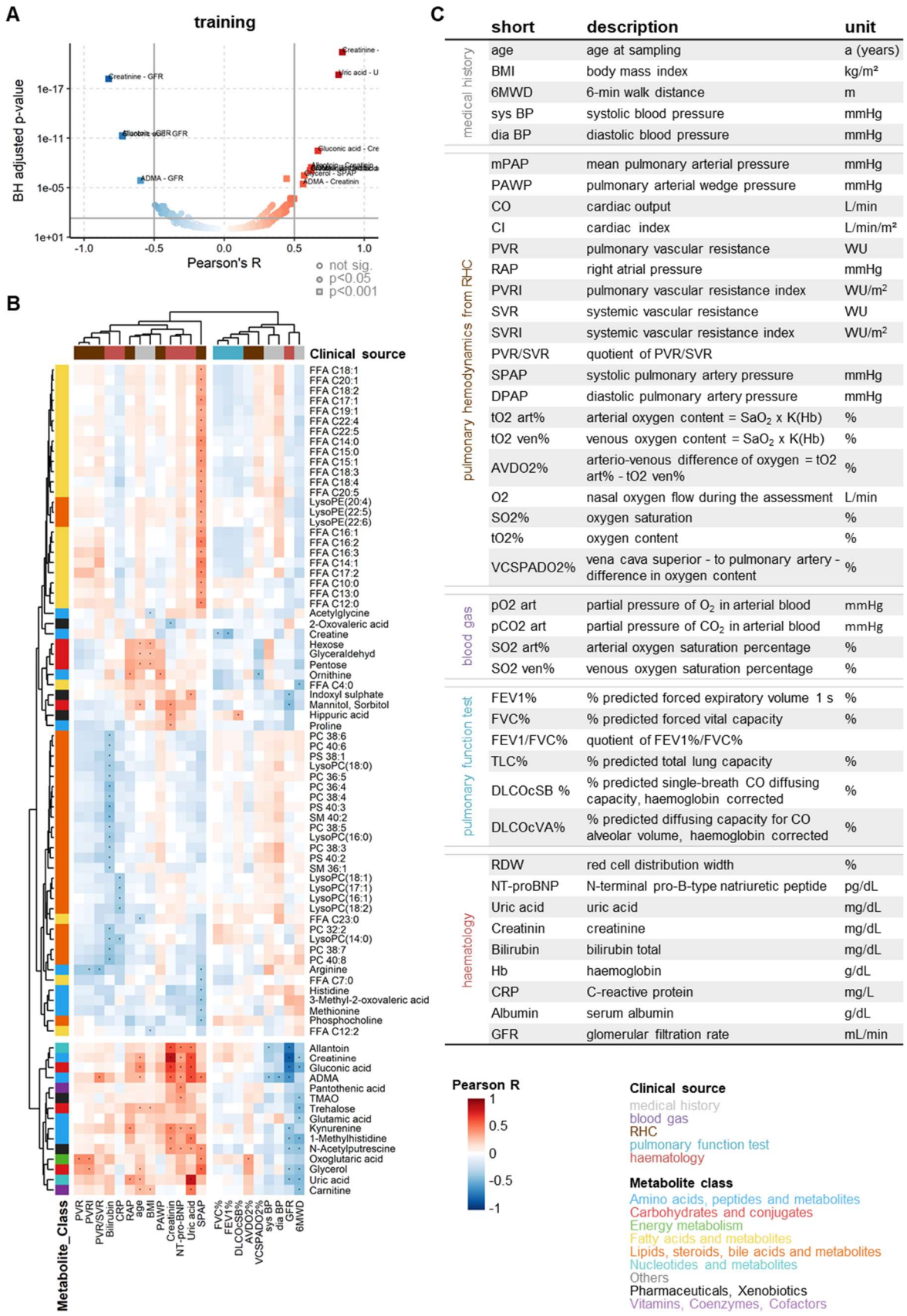

C

	short	description	unit
medical history	age	age at sampling	a (years)
	BMI	body mass index	kg/m²
	6MWD	6-min walk distance	m
	sys BP	systolic blood pressure	mmHg
	dia BP	diastolic blood pressure	mmHg
pulmonary hemodynamics from RHC	mPAP	mean pulmonary arterial pressure	mmHg
	PAWP	pulmonary arterial wedge pressure	mmHg
	CO	cardiac output	L/min
	CI	cardiac index	L/min/m²
	PVR	pulmonary vascular resistance	WU
	RAP	right atrial pressure	mmHg
	PVRI	pulmonary vascular resistance index	WU/m²
	SVR	systemic vascular resistance	WU
	SVRI	systemic vascular resistance index	WU/m²
	PVR/SVR	quotient of PVR/SVR	
	SPAP	systolic pulmonary artery pressure	mmHg
	DPAP	diastolic pulmonary artery pressure	mmHg
	tO2 art%	arterial oxygen content = SaO_2 x K(Hb)	%
	tO2 ven%	venous oxygen content = SaO_2 x K(Hb)	%
	AVDO2%	arterio-venous difference of oxygen = tO2 art% - tO2 ven%	%
	O2	nasal oxygen flow during the assessment	L/min
	SO2%	oxygen saturation	%
	tO2%	oxygen content	%
	VCSPADO2%	vena cava superior - to pulmonary artery - difference in oxygen content	%
blood gas	pO2 art	partial pressure of O_2 in arterial blood	mmHg
	pCO2 art	partial pressure of CO_2 in arterial blood	mmHg
	SO2 art%	arterial oxygen saturation percentage	%
	SO2 ven%	venous oxygen saturation percentage	%
pulmonary function test	FEV1%	% predicted forced expiratory volume 1 s	%
	FVC%	% predicted forced vital capacity	%
	FEV1/FVC%	quotient of FEV1%/FVC%	
	TLC%	% predicted total lung capacity	%
	DLCOcSB %	% predicted single-breath CO diffusing capacity, haemoglobin corrected	%
	DLCOcVA%	% predicted diffusing capacity for CO alveolar volume, haemoglobin corrected	%
haematology	RDW	red cell distribution width	%
	NT-proBNP	N-terminal pro-B-type natriuretic peptide	pg/dL
	Uric acid	uric acid	mg/dL
	Creatinin	creatinine	mg/dL
	Bilirubin	bilirubin total	mg/dL
	Hb	haemoglobin	g/dL
	CRP	C-reactive protein	mg/L
	Albumin	serum albumin	g/dL
	GFR	glomerular filtration rate	mL/min

Fig. S3. Selected metabolites correlate with clinical parameters in the training cohort. (A) Volcano plot of all pairwise Pearson correlations of all 164 metabolites (drift corrected, log_{10}-transformed data) versus 43 clinical parameters

highlighting strong (absolute $R > 0.5$, grey vertical lines) and significant ($p_{BH} < 0.05$, grey horizontal line) correlations. Based on training cohort (n = 169). **(B)** Heatmaps with hierarchical clustering of the respective metabolite vs. clinical parameter. Pearson correlations were filtered to keep only rows and columns with at least one sig. correlation. Uric acid and creatinine were measured as metabolite and were part of routine hematology. These are accordingly the strongest, most significant correlations. **(C)** Overview of all investigated numeric clinical parameters correlated in (A, B) with all metabolites, listing their short names, explanations and units.

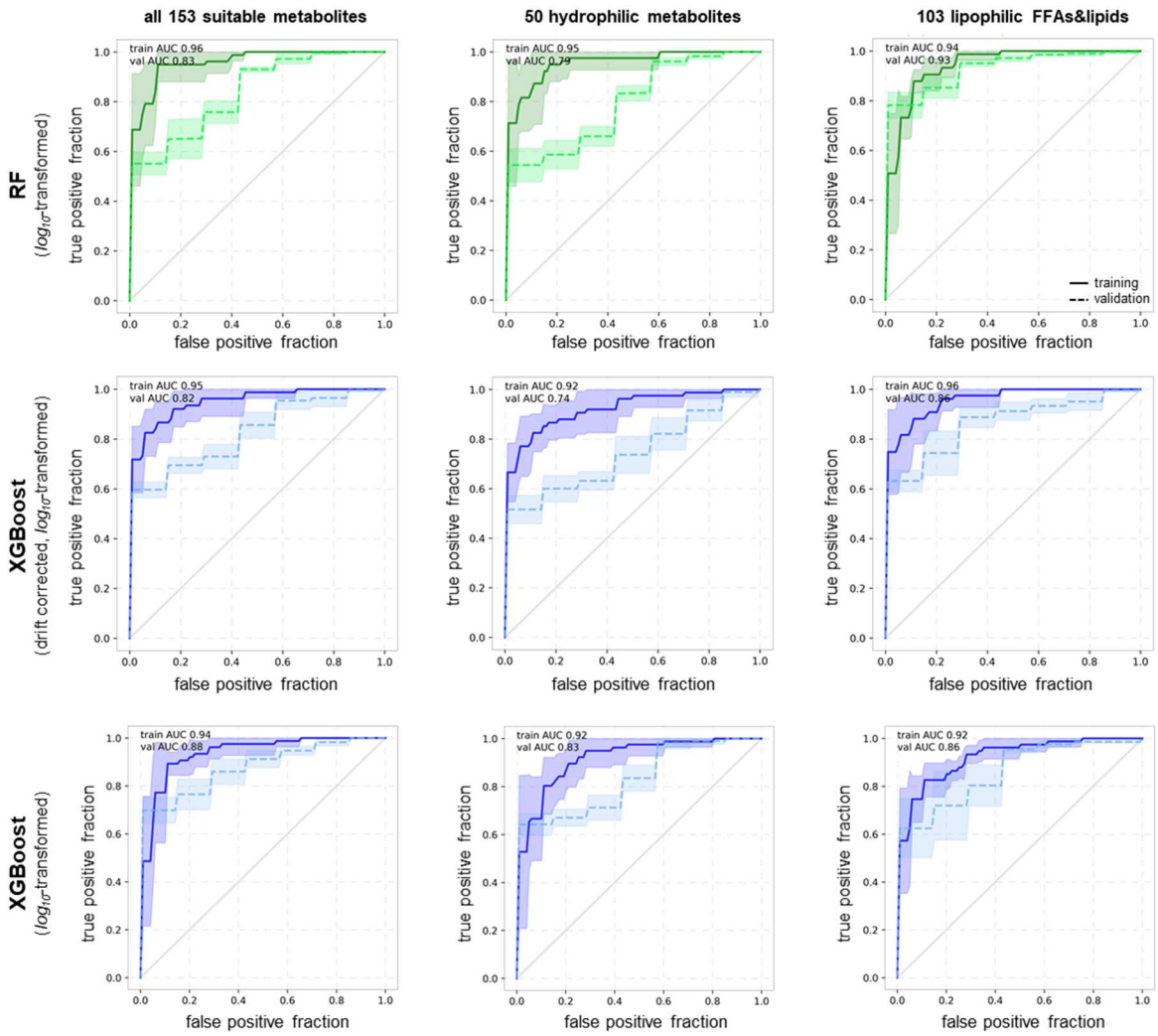

Fig. S4. RF and XGBoost perform similarly with and without drift correction. ROC plots within the training cohort (n = 169, solid lines) and the validation cohort (n = 64, dashed lines) with their 95% confidence intervals as ribbons. For modelling, the training cohort was randomly split into 80% training and 20% testing data. The split was repeated five times without overlap of test data for cross-validation. Top row shows performance of RF without drift correction. The second and third row show the performance of XGBoost with and without drift correction, respectively. Models used either all suitable 153 metabolites (left), only 50 hydrophilic metabolites (middle), or only 103 lipophilic metabolites (right).

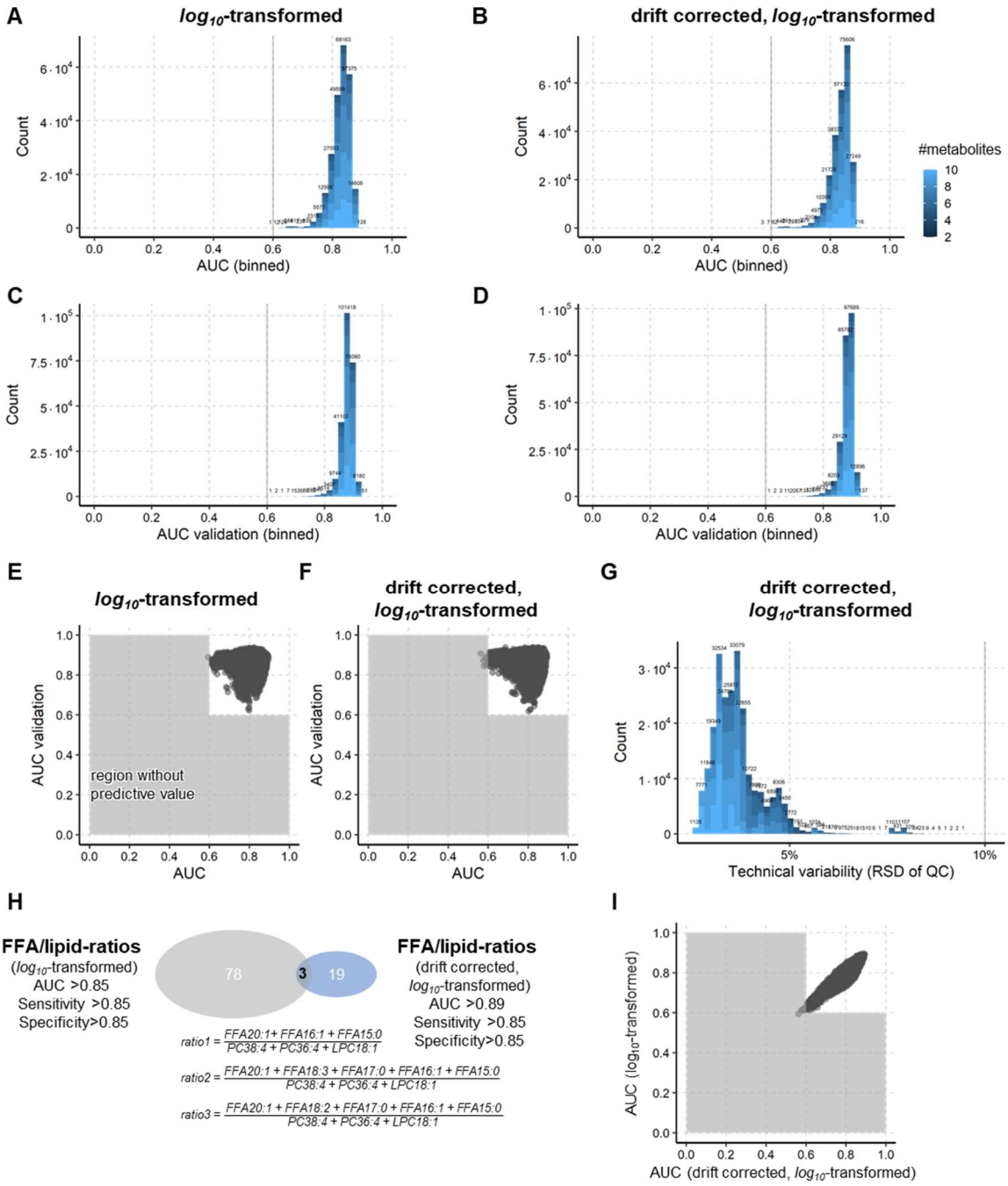

Fig. S5. A quarter million of FFA/lipids-ratios could diagnose PH. (A, B, C, D) The histogram of ROC analysis performance AUC for all possible FFA/lipid-ratios exhibits a tight distribution showing that all ratios performed similarly good. Ratios were calculated from 11 different FFA (numerator) and 8 different lipids (denominator). All possible sums for numerator and denominator were tested, limiting to a maximum of 6 FFA in the numerator and 4 lipids in the denominator yielding a total of 246 842 ratios. The grey vertical line marks an AUC of 0.6 as cut-off for minimal diagnostic performance. ROC analysis was based on the training cohort (n = 169) and benchmarked against the validation cohort (n = 64). **(A, C)** Ratios based on not drift corrected, only log_{10}-transformed data performed all consistently very well, with most achieving around AUC > 0.8. **(B, D)** Drift correction further slightly improved diagnostic performance of the FAF/lipid ratios. **(A, B)** All samples from the trainings data set (cohort 1, 2, 3 with n = 167) were used. **(C, D)** All samples from the validation data set (cohort 4, n = 64) were used. The distribution of ratio performance between trainings data **(A, C)** and validation data **(B, D)** was similar for all ratios.

(E, F) Direct comparison of ratio performance in trainings data versus validation data in **(E)** log_{10}-transformed data and **(F)** log_{10}-transformed, drift corrected data shows a very good overlap. The grey zones mark an AUC of 0.6 as cut-off for minimal diagnostic performance. **(G)** The histogram of the calculated technical error ratio for each ratio exhibits a tight distribution around 5% total technical relative variability showing. The grey vertical line marks the maximally acceptable technical variability cut-off for measurement methods in clinical routine laboratories. **(H)** Overview of top performing ratios in both data types and ratio equation of the three overlapping ratios. **(I)** Direct comparison of ratio performance in the training data between both data types shows a very good overlap. The grey zones mark an AUC of 0.6 as cut-off for minimal diagnostic performance.

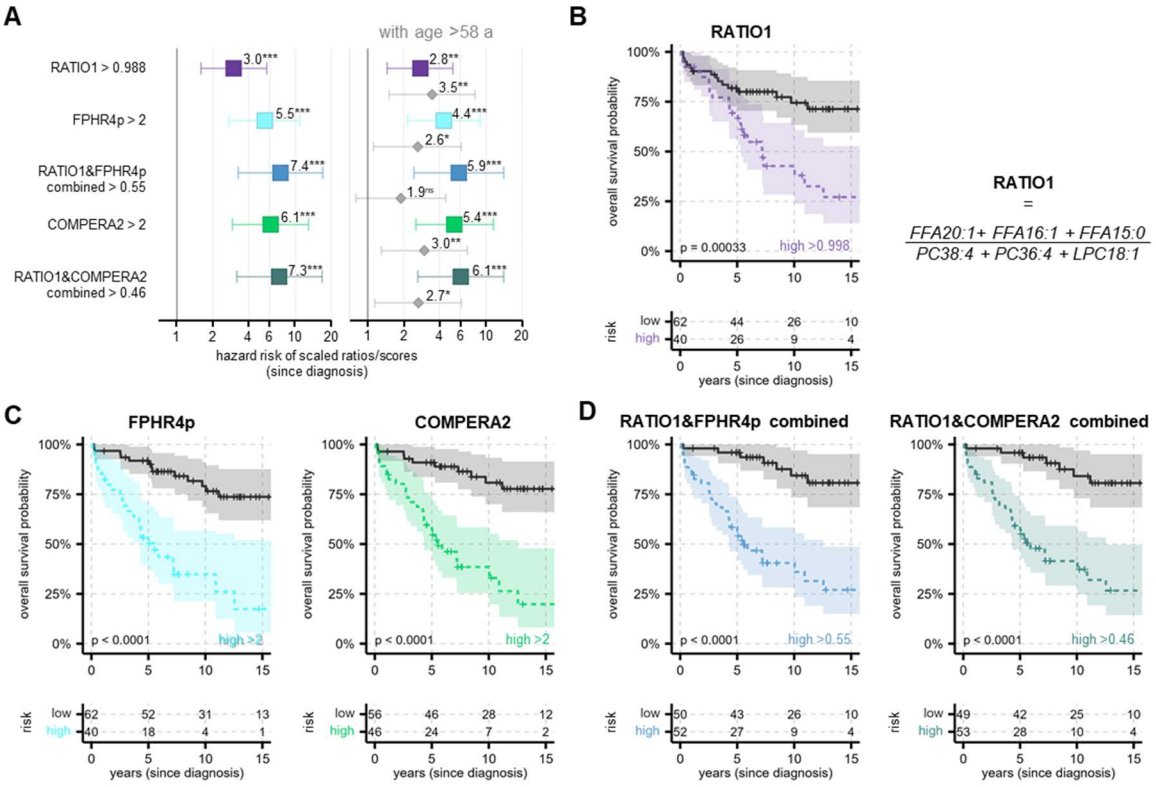

Fig. S6. RATIO1 predicts survival since diagnosis and improves established clinical scores. **(A)** Cox HR analysis for survival since diagnosis and 95% confidence interval with statistical significance coded as not significant (ns); * $p < 0.05$; ** $p < 0.01$; *** $p < 0.001$. Combining RATIO1 with the FPHHR4p or COMPERA 2.0 increased HR compared with scores or RATIO1 alone. **(B, C, D)** Kaplan–Meier curves for survival since diagnosis by RATIO1 **(B)**, FPHR4p and COMPERA 2.0 **(C)** and RATIO1 combined with FPHR4p or COMPERA 2.0 **(D)**. All cut-offs were optimized with maxstat for both Cox HR analysis and Kaplan–Meier analysis. RATIO1 was based on log_{10}-transformed data without drift correction. RATIO1 and scores were combined scaled 0 to 1 to give equal weighing. FPHR4p was inverted so that higher scores also represent higher risk as in COMPERA 2.0 for simpler interpretation.

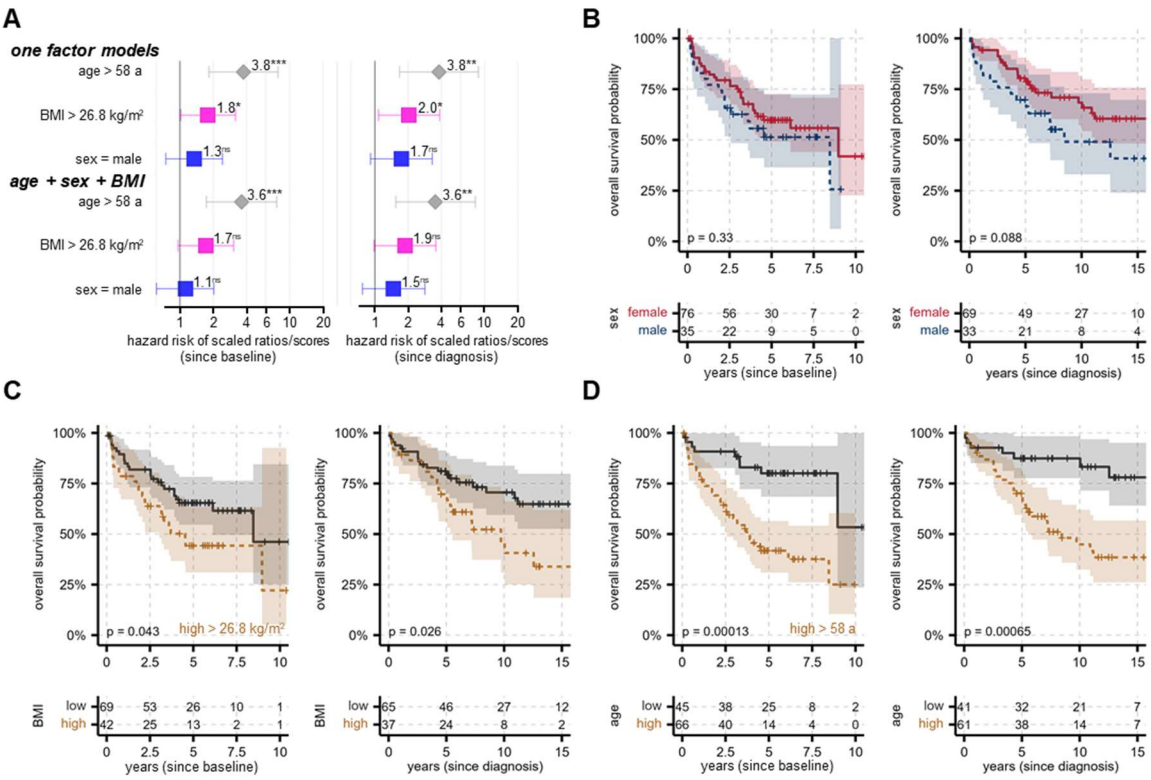

Fig. S7. Survival analysis of covariates age, sex and BMI. (A) Cox HR analysis for survival since baseline (left) and since diagnosis (right) and the 95% confidence interval with statistical significance coded as not significant (ns); * $p < 0.05$; ** $p < 0.01$; *** $p < 0.001$. Higher age alone and in the tri-factor model was a significant risk factor for both times since baseline and times since diagnosis. BMI was barely significant when modelled alone but not significant in the tri-factor model, while sex being male was slightly elevated but never significant. **(B)** Kaplan–Meier curves of survival times since baseline and since diagnosis by age, sex or BMI. Age and BMI cut-offs were optimized with maxstat for both Cox HR analysis and Kaplan–Meier analysis. Survival of PH patients decreases strongly and significantly for higher age and weakly with higher BMI.

930

931

932

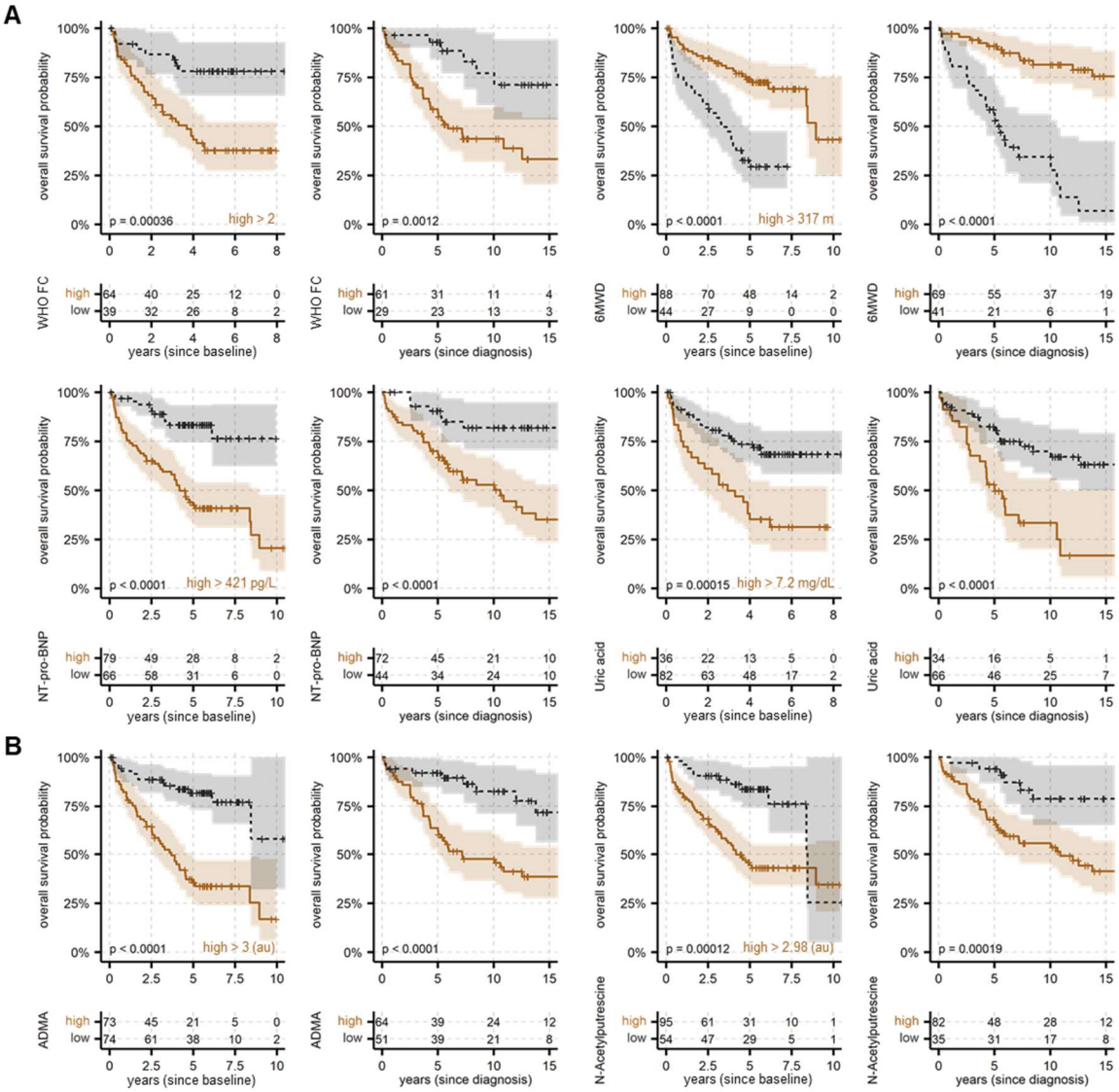

Fig. S8. Further predictors of survival. (A, B) Kaplan–Meier curves analyzing survival times since baseline or since diagnosis for PH patients. The stated cut-off for survival prediction was optimized with maxstat. **(A)** Survival of PH patients significantly decreases with known clinical risk factors such as higher WHO FC classes, lower 6MWD, higher NT-pro-BNP levels, and higher uric acid levels. **(B)** The top two metabolites able to predict survival were ADMA and N-Acetylputrescine (both drift corrected, log_{10}-transformed data) with high levels strongly associated with poor prognosis. All cut-offs were optimized with maxstat for Kaplan–Meier analysis.

933

934 # Supplementary Tables

935 **Table S1: Subject characteristics with medians ± 95% confidence intervals within measurement runs of the training**
936 **cohort**

	run 1		run 2			run 3		
	HC (n=8)	PH (n=8)	HC (n=12)	DC (n=9)	PH (n=12)	HC (n=45)	DC (n=21)	PH (n=52)
Age at sampling, y	57.0±8.8	58.5±9.0	70.5±10.8	56.0±10.1	63.0±9.3	58.0±2.6	60.0±5.7	66.5±3.7
Female:male (ratio)	7:1 (7:1)	7:1 (7:1)	11:1 (11:1)	7:2 (3.5:1)	11:1 (11:1)	26:19 (1.4:1)	13:8 (1.6:1)	30:22 (1.4:1)
BMI kg/m²	22.6±2.7	24.8±3.4	25.8±3.0	30.7±5.5	25.5±3.5	24.1±1.0	22.5±3.2	25.7±1.3
Diagnosis since y	-	3.0±5.9	-	-	6.0±4.0	-	8.0±2.1	0.0±1.1
Pulmonary hemodynamics from RHC								
mPAP (mmHg) mean pulmonary arterial pressure	-	45.0±7.7	-	-	41.5±5.8	-	22.0±0.8[#]	41.0±3.1
PAWP (mmHg) pulmonary arterial wedge pressure	-	10.0±4.2	-	-	5.5±1.7	-	9.5±0.3[#]	10.0±1.6
CO (L/min) cardiac output	-	4.1±1.6	-	-	4.3±0.8	-	3.9±0.4[#]	4.6±0.5
CI (L/min/m²) cardiac index	-	2.3±0.7	-	-	2.5±0.5	-	2.4±0.3[#]	2.6±0.2
PVR (WU) pulmonary vascular resistance	-	8.3±3.7	-	-	8.9±3.1	-	3.2±0.3[#]	6.0±1.2
RAP (mmHg) right arterial pressure	-	5.0±3.8	-	-	5.0±2.4	-	5.0±1.1[#]	7.0±1.5
Clinical data								
6MWD (m) 6-min walk distance	-	338±96	-	-	431±149	-	454±50	317±32
WHO FC world health organisation functional class	-	3.0±0.6	-	-	3.0±0.5	-	2.0±0.3	3.0±0.2
FEV1 (% predicted) forced expiration 1 s	-	83.0±16.5	-	-	82.5±12.9	-	51.5±12	68.5±6.7
FVC (% predicted) forced vital capacity	-	90.9±18.0	-	-	97.6±14.8	-	63.8±8.2	78.0±6.5
FEV1/FVC (% predicted)	-	73.3±6.0	-	-	78.3±6.5	-	56.3±10.3	73.2±3.9
TLC (% predicted) total lung capacity	-	95.7±12.5	-	-	103.1±9.4	-	103.0±13.2	92.0±5.2
DLCO cSB (% predicted) single-breath CO diffusing capacity, hemoglobin corrected	-	69.5±8.4	-	-	65.4±9.5	-	49.6±9.6	56.4±8.2
DLCO cVA (% predicted) CO diffusing capacity alveolar volume, hemoglobin corrected	-	74.6±14.1	-	-	60.6±20.8	-	70.0±9.6	71.0±7.8
RDW (%) red cell distribution width	-	15.5±1.1	-	-	14.4±0.9	-	14.0±0.9	15.7±1.0
NT-proBNP (pg/mL)	-	508±1197	-	-	263±1122	-	90±50	1100±1112.2
Uric acid (mg/dL)	-	5.7±1.4	-	-	5.7±1.6	-	5.0±0.6	6.2±0.7
Creatinine (mg/dL)	-	0.92±0.17	-	-	1.02±0.19	-	0.80±0.11	1.04±0.17
Bilirubin total (mg/dL)	-	0.61±0.25	-	-	0.57±0.26	-	0.40±0.16	0.70±0.17

937 [#]based on 4 patients, not representative

938 **Table S2: Characteristics of patients with IPAH and healthy donors used for laser capture-microdissection of PA.**

	ID	Age	Sex		ID	Age	Sex	mPAP
Donor	1	[50-59]	male	IPAH	1	[30-39]	female	50
	2	[70-79]	female		2	[30-39]	female	88
	3	[50-59]	female		3	[18-29]	female	56
	4	[30-39]	male		4	[18-29]	female	69
	5	[18-29]	female		5	[50-59]	male	66
	6	[50-59]	male		6	[18-29]	male	74
	7	[18-29]	male		7	[50-59]	male	65
	8	[70-79]	female		8	[30-39]	female	69
	9	[50-59]	female		9	[40-49]	male	96
	10	[50-59]	female		10	[18-29]	female	65

939
940
941 **Table S3: Primers used to assess the expression of listed genes.** Gene name, PubMed Nucleotide accession number used
942 for primer design, forward and reverse primer sequences and the size of the PCR product (in bp) 4 are given. All
943 primers were designed so that the PCR product span at least one exon-exon junction.

Gene	Forward primer	Reverse primer	Product size (bp)
SLC25(A5)	GTTGTCGCAGGTGGACTTCT	CCTTACCCTCACAACCTGGC	71
GPAT1	CTGCTAGGGCAGCAGCG	TGCTGGGATGAAAGTTCTTCTGT	108
GPAT2	CTTCCCTTGAGCAGTCCACG	GCCATGAGAGCCTCACACCA	87
AGPAT1	ACAGAGACACAGCCATCCG	CAAATCCATTCTGGCCACCTCAG	102
LIPIN2	TCTCCGCCTTCCACAGAGAA	CTGCTTAGACGGGGCAAACA	98
DGAT1	CAACTACCGTGGCATCCTG	TTCTCCAGAAATAACCGGGC	72

944
945
946 **Table S4: Characteristics of the hPASMC and hPAEC donors used for in vitro studies.**

	ID	Age	Sex		ID	Age	Sex
hPASMC	1	[30-39]	male	hPAEC	1	[50-59]	male
	2	[50-59]	female		2	[40-49]	female
	3	[30-39]	male		3	[50-59]	female
	4	[30-39]	female		4	[50-59]	male
	5	[18-29]	female				
	6	[30-39]	male				

947
948